Miner Deposita (2013) 48:57–79
DOI 10.1007/s00126-012-0412-9

ARTICLE

Refinement of the time-space evolution of the giant Mio-Pliocene Río Blanco-Los Bronces porphyry Cu–Mo cluster, Central Chile: new U–Pb (SHRIMP II) and Re–Os geochronology and $^{40}Ar/^{39}Ar$ thermochronology data

Katja Deckart · Alan H. Clark · Patricio Cuadra · Mark Fanning

Received: 8 September 2011 / Accepted: 8 March 2012 / Published online: 5 April 2012

Abstract Representing one of the largest known (estimated >5 Gt at 1 % Cu and 0.02 % Mo) porphyry system, the Río Blanco-Los Bronces deposit incorporates at least five hypabyssal intrusive and hydrothermal centres, extending for about 5 km from the Río Blanco and Los Bronces mines in the north, through the Don Luis mine, to the Sur Sur mine, La Americana and Los Sulfatos in the south. The new geochronology data, which now include data on different molybdenite vein types, confirm the U–Pb ages of the pre-mineralisation intrusions but slightly increase their age range from 8.8 to 8.2 Ma. The distinct magmatic pulses of the mineralisation-associated porphyritic intrusives (Late Porphyries) indicate an age interval instead of the previously suggested individual ages: the quartz monzonite porphyry ranges from 7.7 to 6.1 Ma (Sur Sur 5.74±0.13 Ma), the feldspar porphyry shows an interval from 5.8 to 5.2 Ma and the Don Luis porphyry from 5.2 to 5.0 Ma. The new Re–Os data on distinct molybdenite vein types confirm the protracted history of Cu(–Mo) mineralisation, inferred previously. The vein development occurred at least from 5.94 to 4.50 Ma, indicating a time-span of 1.5 Ma for the hydrothermal activity. Hydrothermal minerals dated by the $^{40}Ar/^{39}Ar$ method are generally too young to record the age of early, high-temperature mineralisation. The majority of the $^{40}Ar/^{39}Ar$ data in the Río Blanco porphyry cluster record reheating by either the youngest member of the Late Porphyry suite or the post-mineralisation dacite or rhyolite plug formations at around 4.9–4.7 Ma.

Keywords Río Blanco-Los Bronces · Porphyry copper deposits · U–Pb, Re–Os, $^{40}Ar/^{39}Ar$ geochronology · Central Andes · Chile

Editorial handling: T. Bissig

Electronic supplementary material The online version of this article (doi:10.1007/s00126-012-0412-9) contains supplementary material, which is available to authorized users.

K. Deckart (✉)
Departamento de Geología, Universidad de Chile,
Plaza Ercilla 803,
Casilla 12518, Santiago, Chile
e-mail: kdeckart@cec.uchile.cl

A. H. Clark
Department of Geological Sciences and Geological Engineering,
Queen's University,
Kingston, ON K7L 3N6, Canada

P. Cuadra
Corporación Nacional del Cobre de Chile,
Divisíon Andina, Sta. Teresa 513,
Los Andes, Chile

M. Fanning
Research School of Earth Sciences,
Australian National University,
Canberra, ACT 0200, Australia

Introduction

The Río Blanco-Los Bronces mining district, covering a 15 km^2, NNW-SSE—elongated area between latitudes 33°07′45″ and 33°10′20″ South in the V Region of central Chile, incorporates the largest known cogenetic porphyry Cu–Mo deposit cluster (Fig. 1). The Río Blanco, Don Luis and Sur Sur operations of the Andina Division of CODELCO and the Los Bronces mine of Anglo American p.l.c., together produced 448,150 t Cu and 2,163 t Mo in 2009 from an entirely hypogene sulphide resource exceeding 715.4 Mt, grading 0.63 % Cu at a cut-off grade of 0.5 % Cu. Moreover,

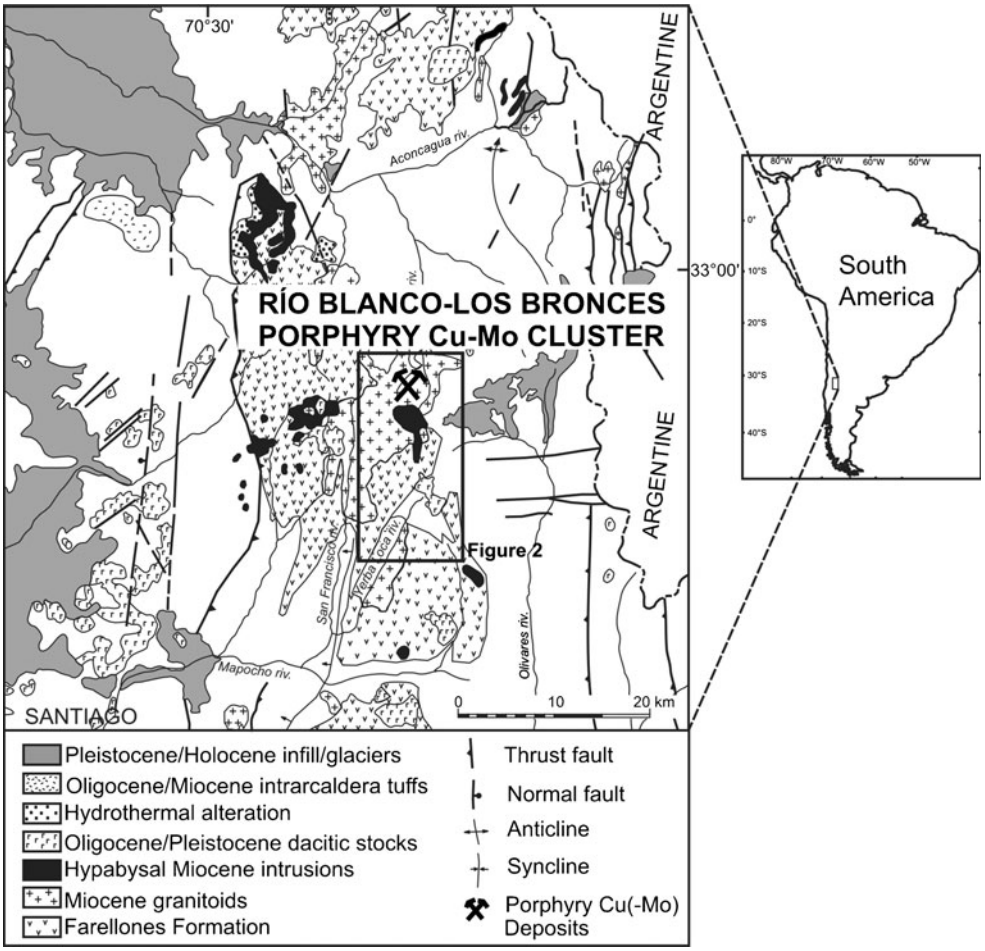

Fig. 1 Simplified geological map of the Río Blanco-Los Bronces megacluster, central Andes. Modified after Rivano et al. (1990) and Deckart et al. (2010)

CODELCO and Anglo American p.l.c. have recently reported major new high-grade drill intersections in, respectively, La Americana and Los Sulfatos sectors at the southern boundary of the cluster (Fig. 2; Mining Journal 2009, p. 3). With its unparalleled three-dimensional exposure in mountainous terrain and in underground and open-pit mines, this enormous concentration of Cu–Mo mineralisation is an excellent locus for the clarification of the ore-genetic and metallogenetic factors responsible for exceptionally fertile magmatic-hydrothermal activity. This goal will, however, require detailed and comprehensive knowledge of the overall temporal and spatial evolution of the undoubtedly complex, polycentred system.

Whereas a latest-Miocene or earliest-Pliocene mineralisation age has been accepted since the K–Ar study of Quirt (1972) and Quirt et al. (1971), supported by numerous K–Ar and, lately, $^{40}Ar/^{39}Ar$ studies (Deckart et al. 2005), considerable ambiguity is evident in the age database. Most critically, Deckart et al. (2005) demonstrated that, at least in the Río Blanco and Don Luis sectors, even ≥95 % $^{40}Ar/^{39}Ar$ plateau ages (PA) for magmatic and hydrothermal micas and alkali feldspars are discordant with respect to isotope dilution - thermal ionization mass spectrometry (ID-TIMS) U–Pb zircon dates for pre- and intra-mineralisation intrusions and record subsequent post-mineral thermal events. On this basis, it was concluded that the unravelling of the age relationships of magmatic and hydrothermal events will require thermally robust, accurate and integrated U–Pb zircon and Re–Os molybdenite geochronology, complemented by $^{40}Ar/^{39}Ar$ incremental-heating thermochronology. The uncertain paragenetic context of the three Re–Os dates reported by Mathur et al. (2001) and the potentially unrepresentative coverage of the U–Pb dates for intra-mineralisation porphyry intrusions presented in our earlier study (Deckart et al. 2005) prompted follow-up research on the ages of intrusion and Cu–Mo mineralisation in all three Andina mining sectors. In this second-stage study, the geochronological database for the Sur Sur centre was significantly expanded and emphasis was placed on the ages of molybdenite-rich veins intersected by drilling below the actively mined intervals of the Andina Division sectors. These new data provide information on the complex time-space relationship and four-dimensional history of intrusion and mineralisation along much of the eastern part of the cluster (Fig. 2).

The major host rocks of the Río Blanco, Don Luis, Sur Sur and, to the south, La Americana hydrothermal centres are stocks of the San Francisco batholith, including (mine geology terminology) the Río Blanco (11.96±0.40 Ma) and Cascada (8.40±0.23 Ma) granodiorites and the Diorite (8.16±0.45 Ma), which intrude thick subaerial andesitic strata of

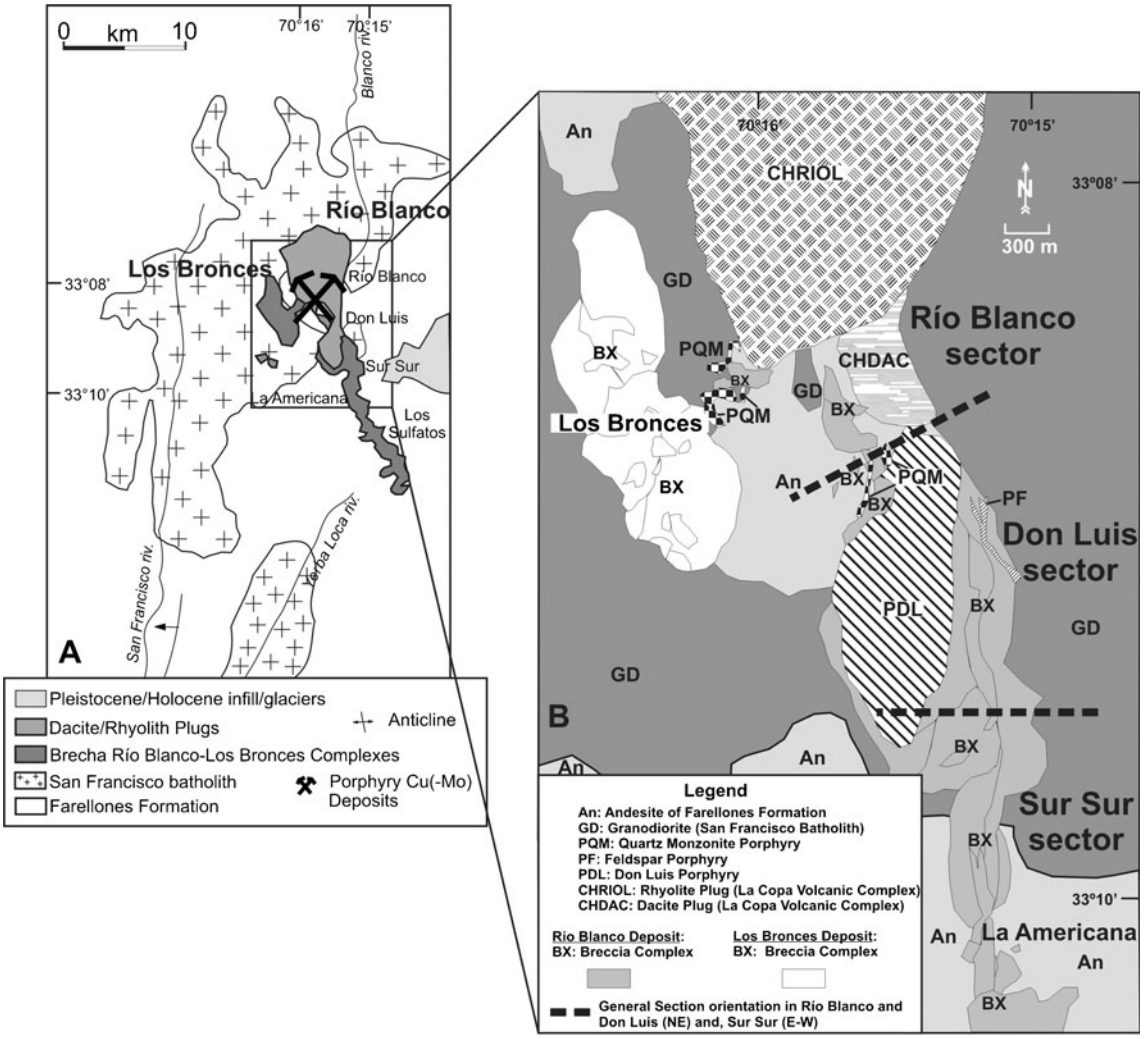

Fig. 2 **a** Simplified geological map showing San Francisco batholith (host rock) in Farellones Formation (pre-intrusive volcanic suite) and Río Blanco-Los Bronces Brecha complexes with post-mineralisation Dacite/Rhyolite plugs. Río Blanco, Don Luís, Sur Sur, La Americana and Los Sulfatos sectors hosting important Cu(–Mo) mineralisation. **b** Simplified geologic map of the Río Blanco-Los Bronces porphyry copper deposit. Modified from Deckart et al. (2005)

the Eocene to earliest Miocene Abanico and overlying mid-Miocene Farellones (16.77±0.25–17.20±0.05 Ma) formations (U–Pb data from Deckart et al. 2005). A significantly older $^{40}Ar/^{39}Ar$ biotite date of 14.8±0.1 Ma has, however, been reported for the Los Bronces quartz monzonite (Munizaga 1994 unpublished report in Serrano et al. 1996) and was confirmed by a zircon U–Pb LA-ICPMS age of 14.7±0.1 Ma (Deckart et al. 2010). Cu–Mo mineralization at Río Blanco, Don Luis and Sur Sur overlapped temporally and spatially with a swarm of granitic porphyry stocks, the "Late Porphyries", traditionally subdivided, from oldest to youngest, into the quartz monzonite, feldspar and Don Luis porphyries, for which U–Pb zircon ID-TIMS dates of 6.32±0.09 (Río Blanco sector), 5.84±0.03 (Don Luis Sector) and 5.23±0.07 Ma (Don Luis Sector), respectively, have been determined (Deckart et al. 2005). Hydrothermal micas associated with mineralised breccia bodies in the wider district yield K–Ar (Serrano et al. 1996) and $^{40}Ar/^{39}Ar$ PA (Skewes, unpublished report; Frikken et al. 2005; Deckart et al. 2005) ranging overall from 14.15 to 4.4 Ma. Both the Late Porphyries and all mineralisation are cut by the La Copa complex, which comprises rhyolitic and dacitic plugs and dykes, as well as tuffs, for which K–Ar and $^{40}Ar/^{39}Ar$ dates of 4.0–4.9 Ma have been reported in Serrano et al. (1996). A similar U–Pb SHRIMP II zircon age of 4.92±0.09 Ma has been determined for the dacite plug, an intrusive unit of this complex (Deckart et al. 2005). A summary of existing recently published age data is given in Table 1.

Table 1 Summary of previously published geochronological data on Río Blanco

Rock unit	Rock type	Dated material	Method	Age (Ma)±2σ	Reference
San Francisco batholith	Río Blanco granodiorite, sector RB	Zircon	U/Pb IDTIMS	11.96±0.4	Deckart et al. (2005)
		Biotite	$^{40}Ar/^{39}Ar$	10.98±0.33	Deckart et al. (2005)
		Biotite	$^{40}Ar/^{39}Ar$	11.59±0.08	Deckart et al. (2005)
	Cascada granodiorite, sector RB	Zircon	U/Pb IDTIMS	8.4±0.23	Deckart et al. (2005)
	Cascada granodiorite, sector DL	K-feldspar	$^{40}Ar/^{39}Ar$	5.25±0.13	Deckart et al. (2005)
		Biotite vein	$^{40}Ar/^{39}Ar$	5.32±0.27	Deckart et al. (2005)
		Biotite vein	$^{40}Ar/^{39}Ar$	4.59±0.11	Deckart et al. (2005)
		Quartz–sericite vein	$^{40}Ar/^{39}Ar$	4.40±0.15	Deckart et al. (2005)
	Diorite, sector DL	Zircon	U/Pb IDTIMS	8.16±0.45	Deckart et al. (2005)
			U/Pb IDTIMS	8.84±0.05	
		Biotite	$^{40}Ar/^{39}Ar$	4.60±0.13	Deckart et al. (2005)
Breccia complex	BXMGD, sector SS	Biotite matrix	$^{40}Ar/^{39}Ar$	4.78±0.04	Frikken et al. (2005)
	BXMGDCC; sector SS	K-feldspar vein	$^{40}Ar/^{39}Ar$	4.67±0.12	Deckart et al. (2005)
	BXT, sector SS	Biotite matrix	$^{40}Ar/^{39}Ar$	5.42±0.09	Frikken et al. (2005)
	Molybdenite breccia	Molybdenite	Re/Os	5.31±0.03	Mathur et al. (2001)
		Molybdenite	Re/Os	5.50±0.03	Mathur et al. (2001)
		Molybdenite	Re/Os	6.26±0.04	Mathur et al. (2001)
Late Porphyries	PQM, sector RB	Zircon	U/Pb IDTIMS	6.32±0.09	Deckart et al. (2005)
	PQM, sector DL	Biotite	$^{40}Ar/^{39}Ar$	4.75±0.10	Deckart et al. (2005)
	PQM, sector RB	Biotite	$^{40}Ar/^{39}Ar$	5.12±0.07	Deckart et al. (2005)
	PDL, sector RB	Zircon	U/Pb IDTIMS	5.23±0.07	Deckart et al. (2005)
	PDL, sector DL	Biotite	$^{40}Ar/^{39}Ar$	4.57±0.06	Deckart et al. (2005)
		Quartz–sericite vein	$^{40}Ar/^{39}Ar$	4.37±0.06	Deckart et al. (2005)
	PF, sector DL	Zircon	U/Pb IDTIMS	5.84±0.04	Deckart et al. (2005)
	PF, sector DL	Biotite	$^{40}Ar/^{39}Ar$	4.62±0.08	Deckart et al. (2005)
La Copa volcanic complex	CHDAC, sector RB	Zircon	U/Pb SHRIMP	4.92±0.1	Deckart et al. (2005)

RB Río Blanco, *DL* Don Luis, *SS* Sur Sur, *BXMGD* magmatic breccias in granodiorite, *BXMDGCC* magmatic breccias in Cascada granodiorite, *BXT* tourmaline breccia, *PQM* quartz monzonite porphyry, *PDL* Don Luis porphyry, *PF* feldspar porphyry, *CHDAC* dacite plug

New geochronological and thermochronological data

New age data are herein presented in sequence for the Río Blanco, Don Luis and Sur Sur sectors, i.e. from north to south (Fig. 2) and for each centre, in terms of decreasing isotopic closure temperature. These are ≤800°C for U–Pb in zircon (Chesley 1999), 550±50°C for Re–Os in molybdenite (Suzuki et al. 1996), 280±20°C for $^{40}Ar/^{39}Ar$ in biotite (Dodson 1973) and 175–220°C for $^{40}Ar/^{39}Ar$ in K-feldspar (Harrison and McDougall 1982). Analytical procedures are summarised in ESM Text 1 and full data are given in ESM Tables 2, 3 and 4.

The mineralogy of molybdenite-bearing veins and their alteration envelopes, summarised in Table 2 and presented in Fig. 3, permits assignment to the categories defined originally for the El Salvador deposit by Gustafson and Hunt (1975; i.e. A, B and D vein types) and Gustafson and Quiroga (1995; C-type). However, Andina Division mine geologists employ a vein classification which highlights observed cross-cutting relationships rather than mineralogy. Veins dated herein by Re–Os methods are described in terms of both mine and El Salvador-based terminology. A macroscopic description of each analysed molybdenite vein is given in Table 3.

It should be emphasised that although the dated molybdenite-bearing veins embrace the transition from alkali-metasomatic (K and Na) to hydrolytic, largely phyllic, alteration and from sinuous to hydrolytic/planar geometries, recording the "Late-Magmatic-to-Hydrothermal" evolution (e.g. Frikken et al. 2005; Cannell et al. 2005), the earliest veins distinguished by Andina geologists, that are Early Biotite ("EB"), "K-feldspar" and "transitional from Early Biotite to A-type" are unrepresented in our Re–Os database. The latter dates therefore largely document the Transitional to Late stages of the porphyry systems (sensu Gustafson and Hunt 1975). Furthermore, a considerably older, presumably minimum $^{40}Ar/^{39}Ar$ date of 14.14 Ma for hydrothermal biotite in the cement of a breccia in the small Los Machos centre (Skewes, unpublished report) indicates that our new age data document the major, terminal events in the evolution of the cluster.

Table 2 Molybdenite vein characteristics of El Salvador and Río Blanco

Vein type	El Salvador (Gustafson and Hunt 1975; Gustafson and Quiroga 1995)	Río Blanco (mine geologists)
Early		
"EB" veins	bio with varying portions of alb, K-spar, green ser, anh, act; w/wt mag and sulf; no qz; fine-grained, no alteration halo	Fine grained; bio or bio-qz. w/wt bio halo; association with bor and cpy
"A" veins	qz-k-spar-anh-sulf; rare traces of bio; K-spar halos; no symmetry; cpy-bor; traces of moly	Sinuous veins; discontinuous granular qz with bor and cpy; halos of K-spar and/or alb
Transitional		
"B" veins	qz-anh-sulf; coarse qz; k-spar absence; symmetry sulf-anh along centrelines; lack of alteration halos; moly-cpy assemblage; veins are reused by later vein events	Generally without alteration halo or with millimetric alb; with moly, cpy, py; symmetric with centreline; veins are re-used by later vein events
"C" veins	Dark micaceous vein with sericitic halo; abundant sulf with green ser, bio, anh, less qz; py, cpy-py, cpy-bor w/wt moly and mag; halos with alkali-feldspar, green ser, bio, chl, anh, anda, sphene	qz-sulf with bio, chl; or only sulf; alteration halos grey-green to dark green with bio-chl, chl-ser assemblages; green ser
Late		
"D" veins	sulf-anh with minor qz; carb. possible; feldspar destructive halos; ser or ser-chl halos w/wt kaol-calc halos; py predominant; cpy, bor, enar, ten, sphal, gal common; minor moly; reaction textures typical	Centerline py-cpy with minor qz; alteration halo of qz-ser; light colored by ser-kaol presence; halos with zonation from centreline to outside: ser-kaol-chl-smec; common presence of carb-tourm
"E" veins	–	Similarity with "D" veins; except of presence of cal-ank-side (carbonates) in halo and centreline; gal-sphal-enar.-salts-py-yeso at tourmaline breccias

EB early biotite, *bio* biotite, *alb* albite, *K-spar* potassic feldspar, *ser* sericite, *anh* anhydrite, *mag* magnetite, *sulf* sulfate, *qz* quartz, *bor* bornite, *cpy* chalcopyrite, *moly* molybdenite, *py* pyrite, *chl* chlorite, *anda* andalusite, *carb* carbonate, *cal* calcite, *kaol* kaolinite, *enar* enargite, *ten* tennantite, *sphal* sphalerite, *gal* galena, *smec* smectite, *tourm* tourmaline, *ank* ankerite, *w/wt* with or without

A global summarised sample description of all geochronologically analysed samples is presented in ESM Tables 5, 6 and 7.

Río Blanco sector

U–Pb data Five new SHRIMP II ablation dates were determined for Late Porphyry intrusions in this sector (Table 4; Figs. 2 and 4a–e; ESM Tables 2 and 5). Three separates from the oldest unit, the quartz monzonite porphyry, representing a vertical interval of 900 m, yielded weighted mean ages of 6.64±0.38 Ma (mean square weighted deviation (MSWD)=0.56; DDH806, 514–520 m; Fig. 4a), 6.16±0.11 Ma (MSWD=1.5; Segment CP-63, level 16 1/2; Fig. 4b) and 7.12±0.19 Ma (MSWD=0.58; DDH786, 889.7–905 m; Fig. 4c), respectively. The two younger dates are concordant with the published ID-TIMS data (Table 1), but the oldest is significantly older although overlapping in error with the age for the DDH806 sample. A sample representative of the youngest of the three porphyry suites, the Don Luis porphyry, gave a new weighted mean age of 5.08±0.16 Ma (n=16; MSWD=1.17; Fig. 4d), essentially concordant with an ID-TIMS date for a sample from the same lithological unit in the Don Luis sector (Deckart et al. 2005). In addition to the above new dates for the Late Porphyries, a U–Pb date has been determined for zircon from the Rhyolite plug of the La Copa complex (DDH459; 236–238 m; Figs. 2b and 4e). The analysis yielded a bimodal pattern, with two weighted mean ages of 4.69±0.23 Ma (n=13; MSWD=1.9) and 11.5±0.3 Ma (n=9; MSWD=0.76). The older date presumably records incorporation of xenocrysts from the Río Blanco granodiorite, but the younger age falls within the range of published K–Ar and U–Pb dates for the complex (e.g. Quirt et al. 1971; Warnaars et al. 1985; Deckart et al. 2005).

Re–Os data Molybdenites from two veins from the Río Blanco sector yielded statistically differing ages of 5.94±0.03 (DDH786; 254.5 m) and 4.89±0.02 Ma (DDH786; 940 m) (Tables 3 and 4). Of these, the older vein, cutting the biotitic cement of a hydrothermal breccia, exhibits the assemblage quartz–chalcopyrite–molybdenite–K-feldspar, and an envelope of sericite and relict K-feldspar, whereas the younger, cutting the quartz monzonite porphyry, lacks chalcopyrite. Although assigned to the B-vein category by Andina, both veins are sinuous, neither shows the characteristic "B"-vein comby quartz structure with a central sulphide seam, and both exhibit more intense sericitisation than

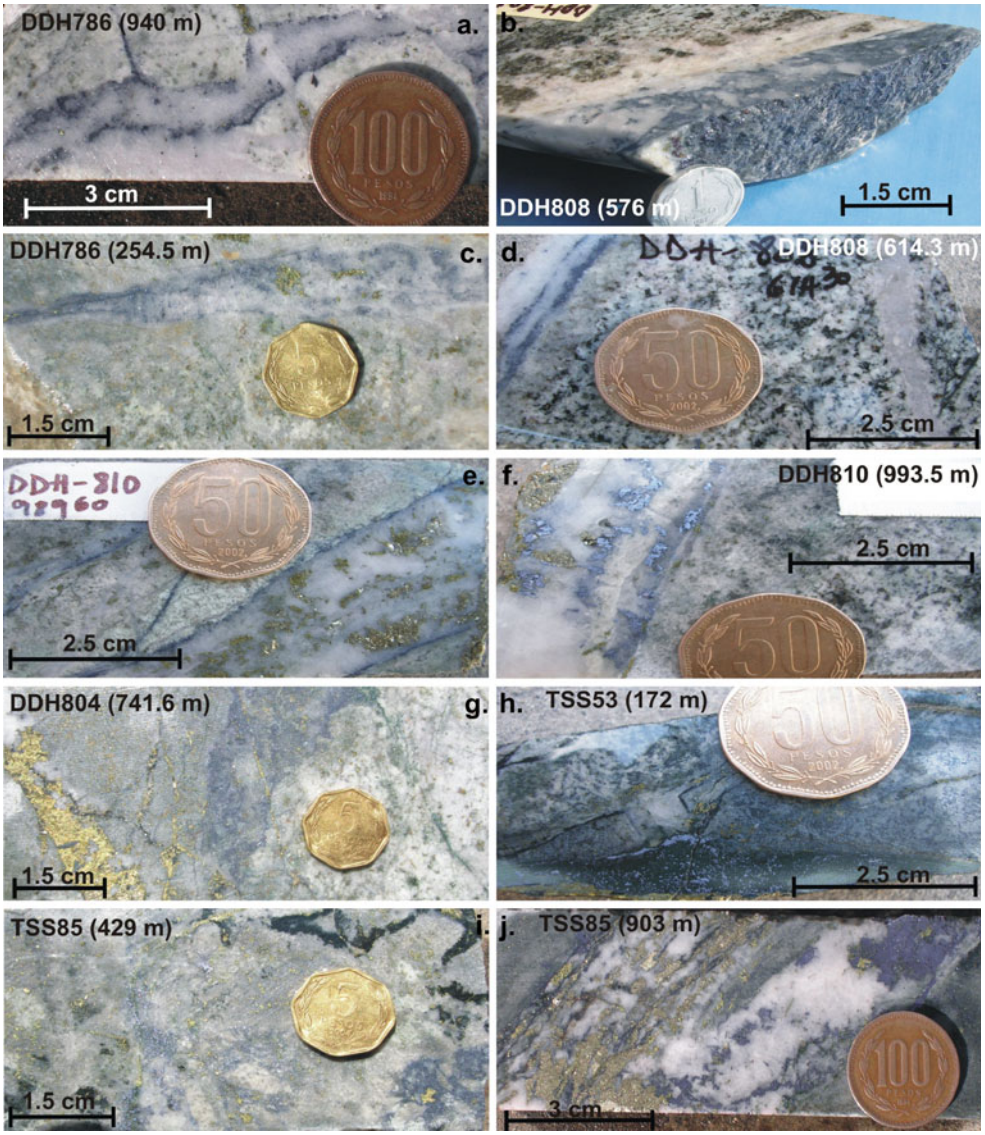

Fig. 3 Molybdenite images from analysed rock specimens. **a**–**d** B-type veins, **d**–**f** C-type veins and **g**–**i** B/D- and **j** E-type veins. All vein types are identified according to Andina geological nomenclature

is typical for B veins (Fig. 3a, c) (Gustafson and Hunt 1975). The 5.94 to 4.89 Ma interval, therefore, is inferred to include two different vein events ("A"- and "B"-type) associated with the intrusion of the quartz monzonite porphyry and the Don Luis porphyry, respectively, in the intermediate and deep levels of the Río Blanco sector.

$^{40}Ar/^{39}Ar$ data Ten samples of host-rocks, hydrothermal breccia cements and veins have been analysed using various $^{40}Ar/^{39}Ar$ techniques such as step-heating and spot-fusion (Table 4; ESM Table 5; Figs. 5 and 6). The oldest age was determined for unaltered hornblende from the Río Blanco granodiorite (DDH173; 30 m; Fig. 5a). The PA of 11.2±0.4 Ma (MSWD=1.57) is concordant with the less precise inverse-isochron age (IIA) of 11.7±1.1 Ma (MSWD=1.60; $^{40}Ar/^{36}Ar$=290±12), and slightly younger than, but within error of, the U–Pb date for this unit.

Three biotites and a single K-feldspar were analysed from the cement of a "magmatic breccia" (mine terminology) body, with inherent chalcopyrite mineralisation, cutting the Río Blanco and Cascada granodiorite units of the San Francisco batholith over a vertical interval of 200 m. Two biotite samples yielded PA of, respectively, 5.33±0.15 Ma (DDH803A, 828.4 m; MSWD=0.57; IIA=5.31±0.17 Ma (MSWD=0.59); $^{40}Ar/^{36}Ar$ intercept 298±11) and 4.27±0.12 Ma (DDH786, 933 m; MSWD=1.18; IIA=4.36±0.16 Ma (MSWD=1.04); $^{40}Ar/^{36}Ar$ intercept=289±8) (Fig. 5b, c). A third biotite sample (DDH785, 278 m), however, gave a considerably older weighted mean spot-fusion age (WMA) of 9.47±0.80 Ma (MSWD=0.66) and an inverse-isochron age of 5.48±1.14 Ma (MSWD=0.63) with an elevated $^{40}Ar/^{36}Ar$ intercept of 319±4 (Fig. 6a). Of the two dated hydrothermal K-feldspars, one (DDH803A, 470 m) gave a PA of 4.72±0.10 Ma (MSWD=1.47) and a

Table 3 Macroscopic description of molybdenite samples

"B" vein (Late Magmatic to Transitional)	
DDH786 (940 m); Río Blanco	Quartz suture vein with molybdenite rim, sinuous vein; molybdenite vein cut by quartz–chalcopyrite vein
DDH786 (254.5 m); Río Blanco	Irregular quartz–chalcopyrite–molybdenite vein with sericite–potassic feldspar halo; molybdenite on rim with potassic feldspar (sericite) halo
DDH808 (614.3 m); Don Luís	Quartz–molybdenite vein; regular halo of potassic alteration
DDH808 (576 m); Don Luís	Quartz–molybdenite vein; strong potassic alteration halo
"C" vein (early hydrothermal)	
TSS53 (172 m); Sur Sur	Irregular quartz–molybdenite vein; chlorite halo; vein associated with pyrite
DDH804 (741.6 m); Don Luís	Irregular molybdenite vein associated with pyrite-chlacopyrite-(bornite); irregular sericite-chlorite rim
TSS85 (429 m); Sur Sur	Irregular molybdenite vein associated with pyrite-chalcopyrite-(bornite); irregular sericite-chlorite rim
"B" or "D" vein (Late Magmatic to Transitional or Main Hydrothermal)	
DDH810 (993.5 m); Don Luís	Quartz–molybdenite-pyrite/chalcopyrite vein; molybdenite in rim and vein centre; sericite halo
DDH810 (989.6 m); Don Luís	Quartz–pyrite–(chalcopyrite) with fine regular rim of molybdenite; reactivation of a molybdenite vein?
"E" vein (Late Hydrothermal)	
TSS85 (903 m); Sur Sur	Quartz–pyrite/chalcopyrite–(chalcosite) coarse molybdenite–quartz vein with wide symmetric quartz–sericite halo

concordant IIA of 4.57±0.16 Ma, with an atmospheric $^{40}Ar/^{36}Ar$ ratio of 304±8 (MSWD=0.85) (Fig. 5d). The second, from a K-feldspar-rich aplite dyke (DDH785, 278 m) gave a spot-fusion WMA of 5.89±0.26 Ma (MSWD=3.15) and an IIA of 5.48±0.40 Ma (MSWD=1.99, with a $^{40}Ar/^{36}Ar$ intercept of 309±12) (Fig. 6b).

All of the $^{40}Ar/^{39}Ar$ ages are younger than the U–Pb dates of the breccia clasts, and, with the exception of the single biotite mean weighted age (MWA) of 9.47 Ma, there is no clear discordance between the dates for biotite and K-feldspar. Further, the $^{40}Ar/^{39}Ar$ ages for "magmatic breccia" cement minerals are younger than the Re–Os date for molybdenite from a vein which cuts the breccia. In other words, the Don Luis porphyry in the Río Blanco sector (5.08–5.23 Ma: this paper and Deckart et al. 2005) and the La Copa rhyolite (4.69 Ma, herein) clearly demonstrate their thermal influence on the entire $^{40}Ar/^{39}Ar$ age range in the Río Blanco sector. In consequence, the $^{40}Ar/^{39}Ar$ data represent resetted and/or secondary mineral ages. Mineral vein ages obtained by spot fusion analysis of a quartz–sericite vein (DDH766, 148–149 m) yielded a WMA of 9.39±0.50 Ma (MSWD=0.86) and a markedly younger IIA of 5.89±0.74 Ma (MSWD=0.95) with a slightly increased $^{40}Ar/^{36}Ar$ intercept of 315±3 (Fig. 6c). This vein cuts a K-feldspar vein (DDH766 (148–149 m)) with a WMA of 5.11±0.13 Ma (MSWD=1.47) and a concordant IIA of 5.08±0.15 Ma (MSWD=1.48; $^{40}Ar/^{36}Ar$ intercept of 299±8) (Fig. 6d). Another spot fusion analysis of a K-feldspar vein (DDH785, 517 m) cutting "magmatic breccia" with granodiorite clasts yielded a WMA of 7.95±0.52 Ma (MSWD=2.10) and a markedly younger IIA of 5.54±0.86 Ma (MSWD=2.60) with an anomalously high $^{40}Ar/^{36}Ar$ intercept of 330±5 (Fig. 6e).

The youngest phyllic alteration age in this sector was obtained for a sericite separate from a vein cutting the Dacite plug of the La Copa complex (XC-155, Level 16 1/2). The total-fusion age of 4.47±0.15 Ma is in conformity with the new U–Pb zircon date for the complex.

Don Luis Sector

U–Pb data SHRIMP II dates were determined for zircons (Fig. 7a) from the diorite unit of the San Francisco batholith, the quartz monzonite porphyry, previously dated from the Río Blanco Sector and the feldspar porphyry. This feldspar porphyry was earlier dated by the ID-TIMS method (Deckart et al. 2005).

A weighted mean age of 8.76±0.23 Ma was calculated for 17 analytical points for the diorite (DDH810 (912–916 m); MSWD=0.67). The quartz monzonite porphyry, DDH807 (724–728 m) yielded a WMA (20 points) of 6.45±0.15 Ma (MSWD=0.72) (Fig. 7b), falling well within the range of 6.16 to 7.12 Ma determined by ID-TIMS (Deckart et al. 2005) and SHRIMP II techniques for samples from the Río Blanco sector.

Twenty analytical points yielded a crystallisation age of 5.17±0.12 Ma (MSWD=1.2) for a zircon separate from a sample of feldspar porphyry from DDH742 (7–13 m) (Fig. 7c). The calculated average age is significantly younger

Table 4 Summary of new U/Pb, $^{40}Ar/^{39}Ar$ and Re/Os ages

Sample	Level (m a.s.l.)	North	East	Rock unit	Sector	Mineral	Age (Ma)	±error (2σ; Ma)	MSWD
DDH806 (514–520 m)	2,755	27,413.74	23,157.81	PQM	RB	Zircon	6.64	0.38	0.56
DDH786 (889.7–903 m)	2,351	27,457.86	23,550.54	PQM	RB	Zircon	7.12	0.19	0.58
Segment CP-36	3,224	NN	NN	PQM	RB	Zircon	6.16	0.11	1.5
Loop Chancador Don Luis	3,132	NN	NN	PDL	RB	Zircon	5.08	0.16	1.17
DDH459 (236–238 m)	3,466	27,978.14	22,996.25	CHRIOL	RB	Zircon	4.69 (11.5)	0.23 (0.3)	1.9 (0.76)
DDH807 (724–728 m)	2,638	27,608.99	24,522.04	PQM	DL	Zircon	6.45	0.15	0.72
DDH742 (7–13 m)	3,184	NN	NN	PF	DL	Zircon	5.17	0.12	1.2
DDH810 (912–916 m)	2,501	26,513.94	23,738.46	Diorite	DL	Zircon	8.76	0.23	0.67
TSS86 (807–809 m)	2,943	25,251	24,429	PQM	SS	Zircon	5.74	0.13	1.08
DDH786 (940 m)	2,349	27,457	23,552	Post-PQM; "B" vein	RB	Molybdenite	4.89	0.02	–
DDH786 (254.5 m)	2,997	27,529.82	23,301.00	BXMGD (fragm. GDRB); "B" vein	RB	Molybdenite	5.94	0.03	–
DDH804 (741.6 m)	2,653	27,646.64	24,008.12	BXMGD (fragm. GDRB); "C" vein	DL	Molybdenite	5.50	0.03	–
DDH808 (614.3 m)	2,729	26,401.37	24,700.54	GDCC "B" vein	DL	Molybdenite	4.76	0.02	–
DDH810 (989.6 m)	2,446	26,468.16	23,703.43	GDCC "B" or "D" vein	DL	Molybdenite	4.50	0.02	–
DDH810 (993.5 m)	2,448	26,470.13	23,704.93	GDCC "B" or "D" vein	DL	Molybdenite	Ø[a] 4.80 4.77 4.83 (4.21)	0.38 0.02 0.02 (0.02)	–
DDH808 (576 m)	2,758	26,426.7	24,685.9	GDCC "B" vein	DL	Molybdenite	4.99	0.02	–
TSS85 (903 m)	2,842	24,955	24,791	GDCC "E" vein	SS	Molybdenite	5.11	0.03	–
TSS85 (429 m)	3,268	25,180.49	24,733.93	BXT (fragm. diorite); "C" vein	SS	Molybdenite	5.79	0.03	–
TSS53 (172 m)	3,465	25,212.09	24,725.87	BXT (fragm. diorite); "C" vein	SS	Molybdenite	5.45	0.03	–
DDH803A (828.4 m)	2,619	NN	NN	BXMGD (fragm. GDRB)	RB	Bio-cement	IIA 5.31	0.17	0.59
DDH786 (933 m)	2,337	27,455.20	23,557.13	BXMGD (fragm. GDRB)	RB	Bio-cement	IIA 4.36	0.16	1.04
DDH803A (470 m)	2,822	27,716.83	23,195.58	BXMGD (fragm. GDCC)	RB	FK-cement	IIA 4.57	0.16	0.85
DDH785 (278 m)	2,985	27,513	23,100	BXMGD (fragm. GDRB)	RB	Bio-cement	IIA 5.48	1.14	0.63
DDH785 (278 m)	2,985	27,513	23,100	BXMGD (fragm. GDRB)	RB	FK-aplite	IIA 5.48	0.40	1.99
DDH785 (517 m)	2,802	27,499	23,245	BXMGD (fragm. GDRB)	RB	FK-vein	IIA 5.54	0.86	2.60
DDH766 (148–149 m)	3,022	25,185	24,866	PQM	RB	qz-FK vein	IIA 5.08	0.15	1.48
DDH766 (148–149 m)	3,022	25,185	24,866	PQM	RB	qz-ser. vein	IIA 5.89	0.74	0.95
DDH173 (30 m)	NN	NN	NN	GDRB	RB	Hornblende	PA 11.22	0.35	1.57
XC-155 level 16 1/2	3,224	NN	NN	CHDAC	RB	Sericite	TFA 4.47	0.15	–
DDH804 (743.5 m)	2,654	27,645.27	24,008.66	BXMGD (fragm. GDCC)	DL	Bio-cement	PA 4.65	0.10	0.50
DDH787 (638 m)	2,596	26,907.39	24,682.44	BXMGD (fragm. GDCC)	DL	Bio-cement	IIA 4.54	0.13	0.42
DDH804 (85.4 m)	3,121	27,245.51	24,234.06	BXMGD (fragm. PDL)	DL	FK-cement	IIA 4.24	0.10	1.01
DDH713 (26–26.5 m)	3,216	26,198	24,559	PDL	DL	qz-ser. vein	IIA 4.87	0.31	0.44
DDH749 (214.2–214.7 m)	3,319	26,612	24,313	BXT	DL	Mica border of qz-py vein	IIA 4.71	0.32	1.19
DDH641 (364.5–367 m)	3,201	26,940	24,815	Diorite	DL	Bio-vein	WMA 6.49	1.13	2.10
DDH641 (160–170 m)	3,184	NN	NN	Diorite	DL	Biotite	PA 4.82	0.04	0.60
TSS84 (145.8 m)	3,521	25,532	24,672	BXT (fragm. GDCC); "C" vein	SS	Bio-vein	IIA 8.82	2.70	0.17
TSS81 (646.3 m)	3,209	24,659.75	24,740.16	BXMGD (fragm. GDCC)	SS	FK-cement	PA 5.14	0.10	0.15
TSS85 (590 m)	3,109	25,102.3	24,756.6	BXT (fragm. GDCC)	SS	FK-vein	IIA 4.74	0.15	0.89
TSS85 (599.8 m)	3,117	25,106.8	24,755.5	BXT (fragm. diorite)	SS	FK-vein	IIA4.95	0.26	1.98
TSS86 (809.7–810.4 m)	2,945	25,253	24,430	GDCC	SS	FK-flooding	PA 4.45	0.14	0.58
TSS84 (616.5 m)	3,114	25,357	24,822	BXMGD (fragm. diorite)	SS	Bio-cement	IIA 4.80	0.18	1.84
TSS22 (705.7 m)	2,940	25,447	24,629	BXMGDCC	SS	FK-vein	IIA 4.42	0.88	2.97
TSS22 (708.3 m)	2,940	25,447	24,629	BXMGDCC	SS	Bio-cement	WMA 6.13	1.10	10.85
TSS22 (708.3 m)	2,940	25,447	24,629	BXMGDCC	SS	qz-ser. vein	IIA 5.49	0.51	0.79
TSS22 (802 m)	NN	NN	NN	BXMGDCC	SS	FK-vein	PA 4.69	0.08	0.46
TSS53 (553 m)	3,162	25,185	24,866	Diorite	SS	FK-aplite	IIA 5.06	0.14	0.56

[a] Ø=weighted mean age of 4.77±0.02 and 4.83±0.02 Ma

Bio biotite, *FK* K-feldspar, *qz-ser.* Quartz–sericite, *PA* plateau age, *WMA* weighted mean age, *TFA* total fusion age, *IIA* inverse isochron age, *RB* Río Blanco, *DL* Don Luis, *SS* Sur Sur, *GDRB*, Río Blanco granodiorite, *GDCC* Cascada granodiorite, *PQM* quartz monzonite porphyry, *PDL* Don Luis porphyry, *PF* feldspar porphyry, *CHDAC* dacite plug, *CHRIOL* rhyolithe plug, *BXMGD* magmatic breccias in granodiorite, *BXMDGCC* magmatic breccias in Cascada granodiorite, *BXT* tourmaline breccia

than that previously determined by the ID-TIMS method, i.e. 5.84±0.04 Ma (Deckart et al. 2005). Nevertheless, the 20 individual spots indicate a range from 4.6 to 5.9 Ma with an associated error of 2 to 9 % for each age.

Re–Os data Five molybdenite samples have been analysed from the Don Luis sector. One is from a vein classified as C-type (Tables 2 and 3), cutting "magmatic breccia" containing rock fragments of the Río Blanco granodiorite, two represent "B"-type veins and two are from ambiguous "B"- or "D"-type veins cutting the Cascada granodiorite.

The "B"-type veins of samples DDH808 (576 m) (Fig. 3b) and DDH808 (614.3 m) (Fig. 3d) gave ages of 4.99±0.02 Ma and 4.76±0.02 Ma, respectively. Molybdenite from "B"-type or "D"-type veins from the same drill-core (DDH810) but at greater depths, 989.6 m (Fig. 3e) and 993.5 m (Fig. 3f), yielded ages of 4.50±0.02 and 4.80±0.38 Ma, respectively; the latter is a weighted mean age of one sample and its duplicate. The discordant individual ages for calculating the weighted mean are 4.83±0.02 and 4.77±0.02 Ma. "D"-type veins are described by Andina mine geologists as showing centrelines of pyrite–chalcopyrite–(quartz) surrounded by a quartz–sericite halo with presence of kaolinite–smectite–(carbonate). Both above mentioned vein samples cannot unambiguously be assigned to one vein type but exhibit a combination of "B"- and "C"-type characteristics. The fifth vein, a "C"-type molybdenite vein, of drill core DDH804 (sampled at 741.6 m) (Fig. 3g) which represents the transitional and early hydrothermal stage in the general and traditionally used classification of mineralisation cycles yields an age of 5.50±0.03 Ma. The molybdenite vein mineral association is pyrite–chalcopyrite–(bornite) with a chlorite–sericite alteration envelope (Tab. 3). Obtained Re–Os ages are not concordant, neither in their specific vein stage nor in general. Furthermore, the "C"-type vein molybdenite which after the mineralisation cycle should present the stage between "B"- and "D"-type veins represents the oldest age of all analysed molybdenite veins of the Don Luis sector.

Ar–Ar data Four mineral separates and three spot fusion analyses have been processed for the Don Luis sector. One biotite separate (250–300 μm) from the diorite rock unit (DDH641, 160–170 m; Fig. 8a) shows a PA of 4.82±0.04 Ma (MSWD=0.60). The IIA of this biotite sample yields 4.82±0.06 Ma (MSWD=0.72) with an atmospheric $^{40}Ar/^{36}Ar$ ratio of 296±6. Both ages, PA and IIA, are concordant within their errors. Biotite ages are significantly younger than the U–Pb age range of 8.16–8.76 Ma (this paper and Deckart et al. 2005) of this rock unit. Two biotite and one K-feldspar cement samples belonging to the magmatic breccia of the Don Luis sector were analysed. One biotite cement separate of the magmatic breccia containing rock fragments of Cascada granodiorite (DDH804, 743.5 m; Fig. 8b) yielded a PA of 4.65±0.10 Ma with a MSWD of 0.50. The IIA is 4.69±0.13 Ma with an atmospheric $^{40}Ar/^{36}Ar$ ratio of 292±8 (MSWD=0.47). The K-feldspar cement of the magmatic breccia (DDH804, 85.4 m; Fig. 8c) with Don Luis porphyry fragments located about 500 m vertical distance above the former sample shows a younger PA of 4.31±0.10 Ma with a MSWD of 1.60. The calculated IIA of 4.24±0.10 Ma indicates an atmospheric ratio of 300±3 and a MSWD of 1.01. The third sample (DDH787, 638 m; Fig. 8d) is a biotite cement mineral of the magmatic breccia with Cascada granodiorite clasts and yielded a PA of 4.45±0.11 Ma (MSWD=0.91). The calculated IIA is 4.54±0.13 Ma intercepting the $^{40}Ar/^{36}Ar$ ratio at 289±6 (MSWD=0.42). Three spot fusion analyses have been undertaken on three distinct vein associations from which mineral separation was not possible. A slightly chloritised EB vein cutting the diorite rock unit (DDH641, 346.5–347 m; Fig 9a) yielded a WMA from four out of nine ablations of 6.49±1.13 Ma (MSWD=2.10). The calculated IIA on these four spot results gave 6.69±2.40 Ma (MSWD=3.09). The $^{40}Ar/^{36}Ar$ ratio indicates an imprecise but atmospheric intercept at 292±37. Sericite of a symmetric vein with pyrite suture and a broad quartz–sericite halo has likewise been dated by the $^{40}Ar/^{39}Ar$ spot fusion method. The obtained weighted mean age on four out of eight ablation points (DDH713, 26–26.5 m; Fig. 9b) yielded 4.98±0.16 Ma (MSWD=0.51). The IIA is 4.87±0.31 Ma (MSWD=0.44) intercepting the $^{40}Ar/^{36}Ar$ axis at 300±11. A not fully developed mica (fine vermiculite–biotite)-mix border of quartz veins or quartz rims of unidentified lithoclasts in a tourmaline breccia (DDH749, 214.2–214.7 m; Fig. 9c) yielded a WMA of 5.00±0.10 Ma (MSWD=5.44), including eight of eleven ablation points. The IIA is concordant with the WMA of that sample and gave 4.71±0.32 Ma (MSWD=1.19) with an atmospheric $^{40}Ar/^{36}Ar$ ratio of 298±14.

Sur Sur sector

U–Pb data One zircon separate from the quartz monzonite porphyry yields a weighted mean crystallisation age of 5.74±0.13 Ma (MSWD=1.08; core TSS86, 807–809 m) including 21 of 22 analytical points (Fig. 10). The obtained age is the youngest of all U–Pb analyses undertaken on this rock unit which is present in all sectors. It represents a crystallisation age unique to the southernmost sector (Fig. 2).

Re–Os data Three molybdenite veins, two "C"-type and one "E"-type, have been selected for Re–Os analysis in the Sur Sur sector (Fig. 2). "C"-type vein molybdenite of sample TSS53 (172 m) (Fig. 3h) cutting diorite fragments containing tourmaline breccia yielded an age of 5.45±0.03 Ma. The second "C"-vein (TSS85, 429 m; Fig. 3i) likewise cutting Diorite fragments containing tourmaline breccia gave an age of 5.79±0.03 Ma. The vein mineral association indicates

quartz–chalcopyrite–pyrite with disseminated molybdenite and alteration halo of quartz–sericite–chlorite–(biotite) assemblages. According to the mine classification, the "C"-type vein molybdenite is characteristic for an early hydrothermal stage. From the same drill core but at 903 m (about 400 m vertically below the former sample) the Cascada granodiorite rock unit cutting "E"-type molybdenite vein sample (Fig. 3j) was selected and analysed. The obtained age is 5.11±0.03 Ma. The late hydrothermal evolution stage "E"-type chalcopyrite–pyrite–quartz–(chalcocite) vein with a quartz–sericite alteration envelope should represent the youngest observed mineralisation event of all molybdenite veins (Tab.2). However, regarding the entire Re–Os data set that includes earlier vein-types, the "E"-vein is generally older than the majority of earlier vein events.

Ar–Ar data A total of 11 samples, seven step heating (Fig. 11a–g) and four spot fusion analyses (Fig. 12a–d) have been obtained on samples from the southernmost Sur Sur sector (Fig. 2b). Step heated minerals are K-feldspar and biotite, while the ablation technique has been applied to biotite cement and, biotite, quartz–sericite and K-feldspar veins. A K-feldspar aplite identified in the diorite rock unit (drill core TSS53, 553 m) yields a PA of 5.26±0.10 Ma (MSWD=2.09; Fig. 11a). The calculated IIA is 5.06±0.14 Ma (MSWD=0.56) with a slightly elevated $^{40}Ar/^{36}Ar$ ratio of 308±7. The feldspar "flooding" event (nomenclature used by Andina geologists) recognised in the Cascada granodiorite sample (TSS86, 809.7–810.4 m; Fig. 11b) yielded a PA of 4.45±0.14 Ma (MSWD=0.58) and an IIA of 4.40±0.26 Ma (MSWD=0.62; $^{40}Ar/^{36}Ar$ ratio=296±3). Two K-feldspar veins of drill core TSS85 about 10 m vertically apart from TSS86, cutting a tourmaline breccia with Cascada granodiorite (590 m; Fig. 11c) and diorite (599.8 m; Fig. 11d) fragments, are representing similar ages. The K-feldspar vein cutting tourmaline breccia with Cascada granodiorite fragments is cut by a younger not well defined "C"-type quartz–pyrite vein with a broader sericitic halo which was not dated. The K-feldspar vein yielded a PA of 4.85±0.10 Ma (MSWD=1.20) and an IIA of 4.74±0.15 Ma (MSWD=0.89) with a $^{40}Ar/^{36}Ar$ ratio of 302±7. The sample from a vein at 599.8 m (TSS85) yielded a PA of 5.04±0.11 Ma (MSWD=1.88). The IIA of the same steps used for calculating the PA was 4.95±0.26 Ma (MSWD=1.98) with an $^{40}Ar/^{36}Ar$ intercept of 300±13.

The biotite cement of a magmatic breccia containing diorite fragments from drill core TSS84 (616.5 m) yielded a PA of 4.73±0.14 Ma (MSWD=1.94; Fig. 11e). A concordant inverse isochron age of 4.80±0.18 Ma (MSWD=1.84) was obtained. Its $^{40}Ar/^{36}Ar$ intercept is of 290±9. The K-feldspar cement of another magmatic breccia at Sur Sur with fragments of the Cascada granodiorite (TSS81, 646.3 m; Fig. 11f) revealed a PA of 5.14±0.10 Ma (MSWD=0.15) and a concordant IIA of 5.13±0.20 Ma (MSWD=0.17; $^{40}Ar/^{36}Ar$=296±7). The K-feldspar vein of a magmatic breccia with Cascada granodiorite fragments yielded a PA of 4.69±0.08 Ma (MSWD=0.46; Fig. 11g). The inverse isochron with an atmospheric $^{40}Ar/^{36}Ar$ ratio of 299±24 indicated an age of 4.62±0.47 Ma (MSWD=0.53). This K-feldspar vein in this core section is parallel to a relatively symmetric quartz–sericite–pyrite vein. No cross-cutting relationships could be observed.

Ablation on a chloritised biotite cement from a magmatic breccia with Cascada granodiorite clasts (TSS22, 708.3 m; Fig. 12a) revealed an imprecise WMA of 6.13±1.10 Ma with a bad fit of 10.85 (MSWD). The imprecise IIA of 4.25±3.59 Ma was calculated on four of ten spot analyses. This fit (MSWD=12.12) of data points is likewise unacceptable. The $^{40}Ar/^{36}Ar$ ratio of 328±85 indicates excess Ar or other analytical problems as for example ^{39}Ar-recoil. A symmetric quartz–sericite halo around a vein with a pyrite suture cuts the same drill core (TSS22, 708.3 m; Fig. 12b) from which the biotite cement was analysed. A WMA of 6.95±0.52 Ma (MSWD=2.63) was obtained. The calculated inverse isochron (five from nine analytical points) indicates an age of 5.49±0.51 Ma (MSWD=0.79) with a slightly higher than atmospheric $^{40}Ar/^{36}Ar$ ratio of 316±4. A not well developed quartz–K-feldspar vein cuts the magmatic breccia with Cascada granodiorite lithoclasts (TSS22) at 705.7 m (Fig. 12c). The WMA on five of twelve analytical points is 7.30±0.47 Ma (MSWD=1.99). The calculated IIA on these points reveals a significantly younger age of 4.42±0.88 Ma (MSWD=2.97; $^{40}Ar/^{36}Ar$=324±5). The fourth spot fusion analysis on drill core from the Sur Sur sector was done on a intensely chloritised "C"-type vein of a quartz–pyrite–(biotite/chlorite) suture with a diffuse but nearly symmetric border of biotite/chlorite-quartz cutting a tourmaline breccia containing Cascada granodiorite fragments (TSS84, 145.8 m; Fig. 12d). The WMA from seven out of seven analytical points of the "suture" biotite/chlorite composition was 11.30±3.14 Ma (MSWD=1.97). The IIA yielded 8.82±2.70 Ma with a good fit (MSWD) of 0.17. The $^{40}Ar/^{36}Ar$ ratio of 300±2 is atmospheric.

Fig. 4 Tera Wasserburg U/Pb SHRIMP II analyses of **a**–**c** quartz monzonite porphyry, **d** Don Luis porphyry and **e** rhyolite plug. All samples represent the Río Blanco sector. In the histogram, *gray bars* represent number of zircon analyses included and *white bars* and ellipses not included in the age calculation

Discussion

The pre-mineralisation diorite intrusion of the Don Luis sector (Figs. 2b and 13) yields an U–Pb SHRIMP II crystallisation age of 8.76±0.23 Ma. The new age confirms two previously

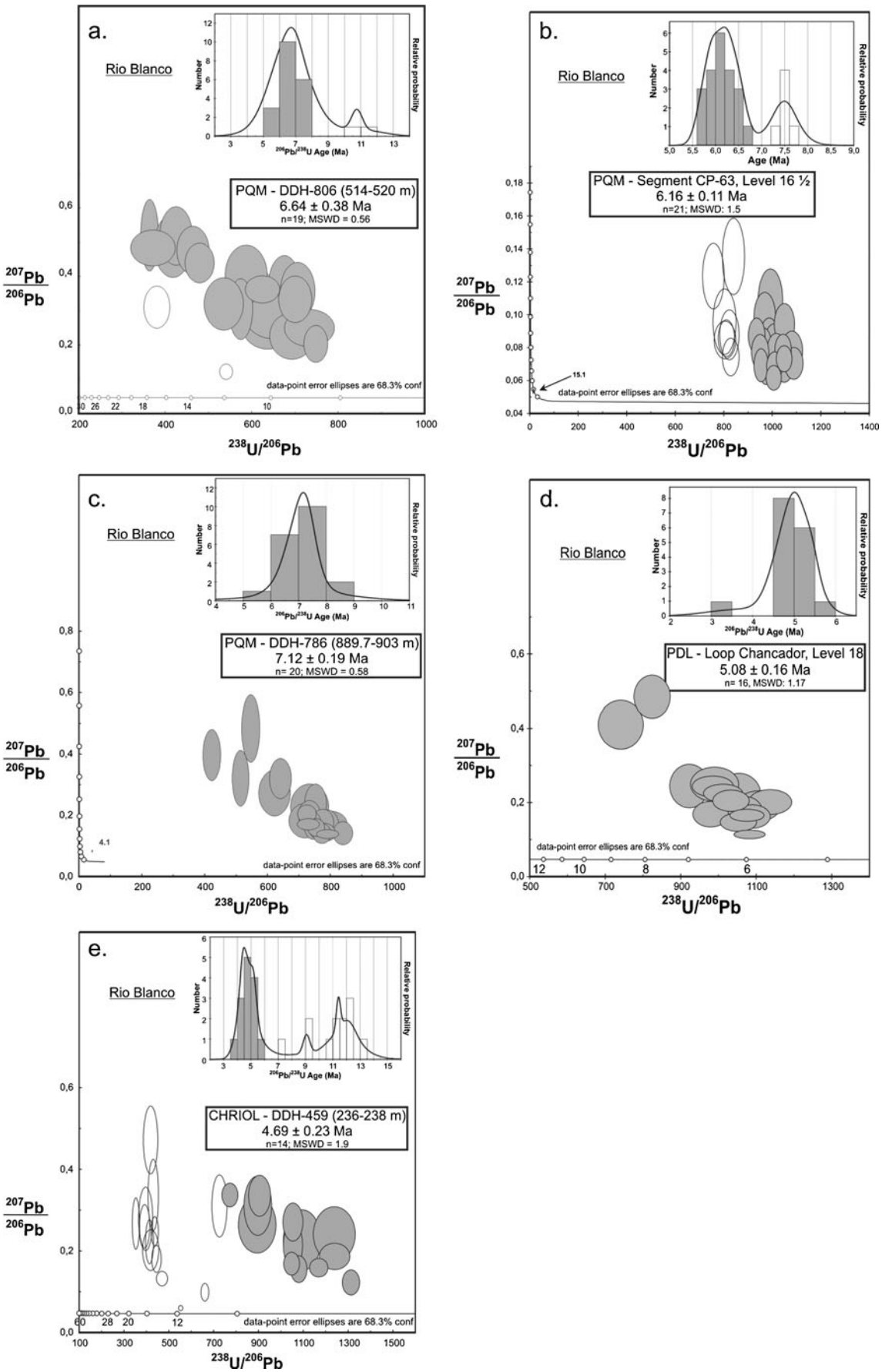
a.
Rio Blanco
PQM - DDH-806 (514-520 m)
6.64 ± 0.38 Ma
n=19; MSWD = 0.56
data-point error ellipses are 68.3% conf
b.
Rio Blanco
PQM - Segment CP-63, Level 16 ½
6.16 ± 0.11 Ma
n=21; MSWD: 1.5
15.1
data-point error ellipses are 68.3% conf
c.
Rio Blanco
PQM - DDH-786 (889.7-903 m)
7.12 ± 0.19 Ma
n= 20; MSWD = 0.58
4.1
data-point error ellipses are 68.3% conf
d.
Rio Blanco
PDL - Loop Chancador, Level 18
5.08 ± 0.16 Ma
n= 16, MSWD: 1.17
data-point error ellipses are 68.3% conf
e.
Rio Blanco
CHRIOL - DDH-459 (236-238 m)
4.69 ± 0.23 Ma
n=14; MSWD = 1.9
data-point error ellipses are 68.3% conf
Number
Relative probability
Age (Ma)
207Pb/206Pb
238U/206Pb

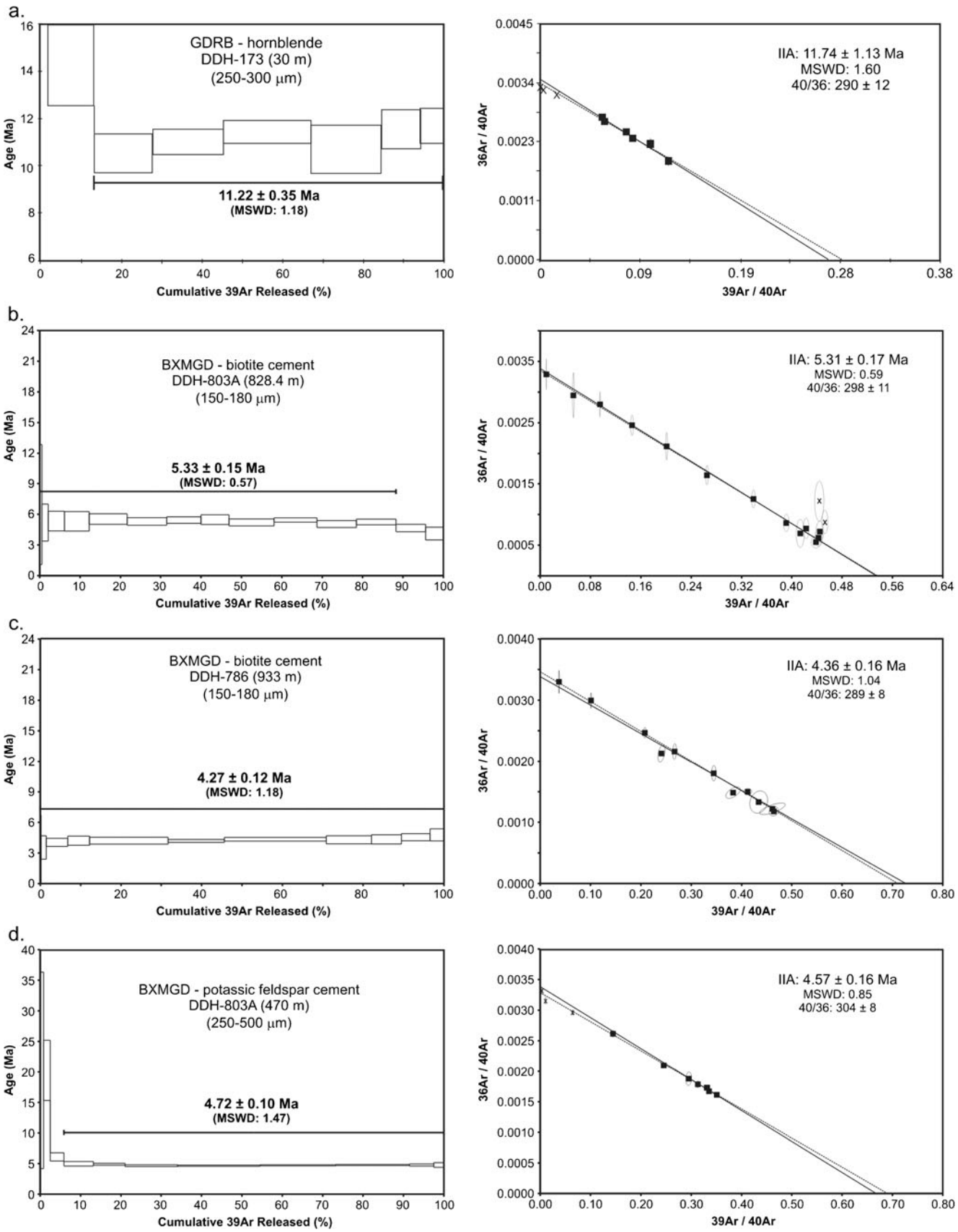

Fig. 5 $^{40}Ar/^{39}Ar$ age spectra and inverse isochron diagrams of **a** Río Blanco granodiorite and **b**–**d** magmatic breccias of the Rio Blanco sector

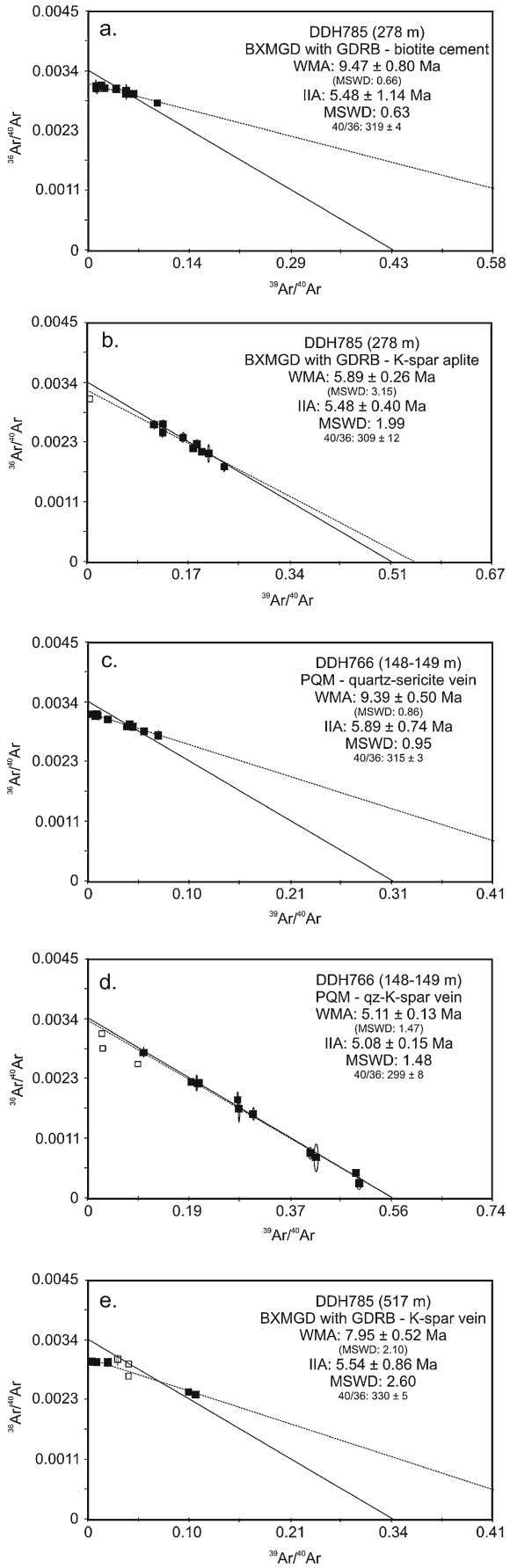

Fig. 6 Inverse isochron diagrams of veins, cement and aplites of the Río Blanco sector. **a** Biotite cement in magmatic breccia, **b** K-feldspar aplite in magmatic breccia, **c** quartz–sericite vein, **d** quartz–feldspar vein in quartz monzonite porphyry and **e**. potassic feldspar vein in magmatic breccia with Río Blanco granodiorite fragments

published ID-TIMS ages of 8.16±0.45 Ma (two single grains) and 8.84±0.05 Ma (zircon fraction) (Deckart et al. 2005). The youngest and the oldest ages are not concordant but the new age indicates concordance between all three obtained data. It is suggested that the age of the diorite intrusion ranges between 8.8 and 8.2 Ma. U–Pb SHRIMP II ages of the Quartz Monzonite porphyry intrusion throughout all sectors reveal similar ranges of crystallisation ages. The new U–Pb SHRIMP II ages (with individual ages ranging from 5.7 to 7.1 Ma) overlap with the previously published U–Pb ID-TIMS age of 6.32±0.09 Ma (Deckart et al. 2005). The youngest and oldest individual ages are visible in the youngest sample (5.74±0.13 Ma; ESM Table 2) which is from the Sur Sur sector (Fig. 2b); the Quartz Monzonite porphyry sample from the Don Luis sector (Fig. 2b) exhibits a bimodal age distribution with a statistical supported 6.2 Ma (n=21 spots) followed by a second peak at 7.5 Ma (n=6 spots). This age range is evident in the entire data set on the quartz monzonite porphyry (ESM Table 2). The U–Pb SHRIMP II age of the feldspar porphyry obtained in this study is slightly younger (5.17±0.12 Ma) compared with the already published ID-TIMS age of 5.84±0.04 Ma (Deckart et al. 2005). It is proposed that the resulting age range for the feldspar porphyry is 5.8 to 5.2 Ma which is shorter and younger than detected for the older quartz monzonite porphyry (Fig. 13). Further, it is suggested that this age range stands for the feldspar porphyry intrusive event. The youngest Don Luis porphyry yields an U–Pb SHRIMP II age of 5.08±0.16 Ma, which is slightly younger but concordant at the 2 sigma error confidence interval compared with the recently published ID-TIMS age of 5.23±0.07 Ma (Deckart et al. 2005). These ages overlap with the lower age range limit of the feldspar porphyry (Fig. 13).

The post-mineralisation rhyolite plug (Fig. 2b) from the La Copa volcanic complex reveals an U–Pb SHRIMP II age of 4.69±0.23 Ma (Fig. 13). This new age coincides with the previously suggested thermal maximum (T>300°C) at 4.6 Ma (Deckart et al. 2005) and might therefore represent the until now unknown heat source in this system. Previous K–Ar biotite and plagioclase ages on the Rhyolite plug range from 4.0 to 4.9 Ma which is concordant with the more precise U–Pb result presented here. The intrusive history in a north-to-south transect through the Río Blanco part of the Cu (–Mo) porphyry mineralisation is rather diachronous throughout the three mineralised sectors.

New Re–Os dates can be statistically grouped between 5.94 and 4.89 Ma, between 5.50 and 4.50 Ma and between

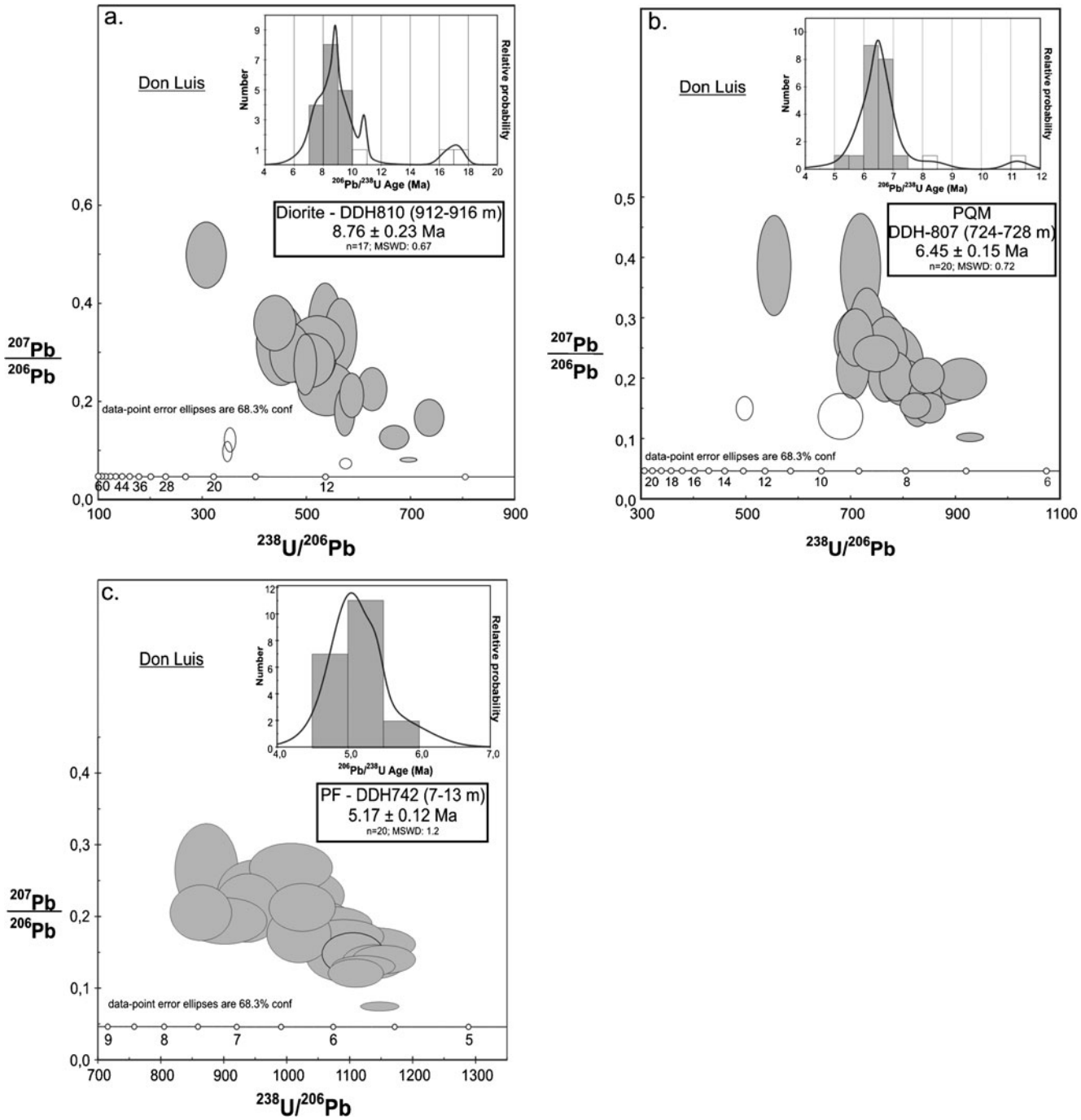

Fig. 7 Tera Wasserburg U/Pb SHRIMP II analyses of **a** diorite, **b** quartz monzonite and **c** feldspar porphyry. All samples represent the Don Luís sector. In the histogram, *gray bars* represent numbers of zircon analyses included and white bars not included in the age calculation

5.79 and 5.11 Ma in the Río Blanco, Don Luis and Sur Sur centres (Figs. 2b and 14a–c), respectively (errors generally are 0.02–0.03 Ma with one exception at 0.38 Ma). The dated veins exhibit textural/mineralogical features characteristic of "B" and "D" veins (cf. Gustafson and Hunt 1975), "C" veins, sensu Dilles and Einaudi (1992), and "E" veins, i.e. high-sulfidation, enargite-bearing structures (cf. Masterman et al. 2005). There are no systematic relationships between vein-types and molybdenite ages, although "C" veins are older than "B" or "D" veins in the Don Luis sector and an "E" vein in Sur Sur. "C" veins in Sur Sur are older than the "E" vein of the same sector. Furthermore, one "B" vein from

Fig. 8 $^{40}Ar/^{39}Ar$ age spectra and inverse isochron diagrams of **a** biotite in diorite, **b** biotite cement, **c** K-feldspar cement and **d** biotite cement in magamatic breccia of the Don Luís sector ▶

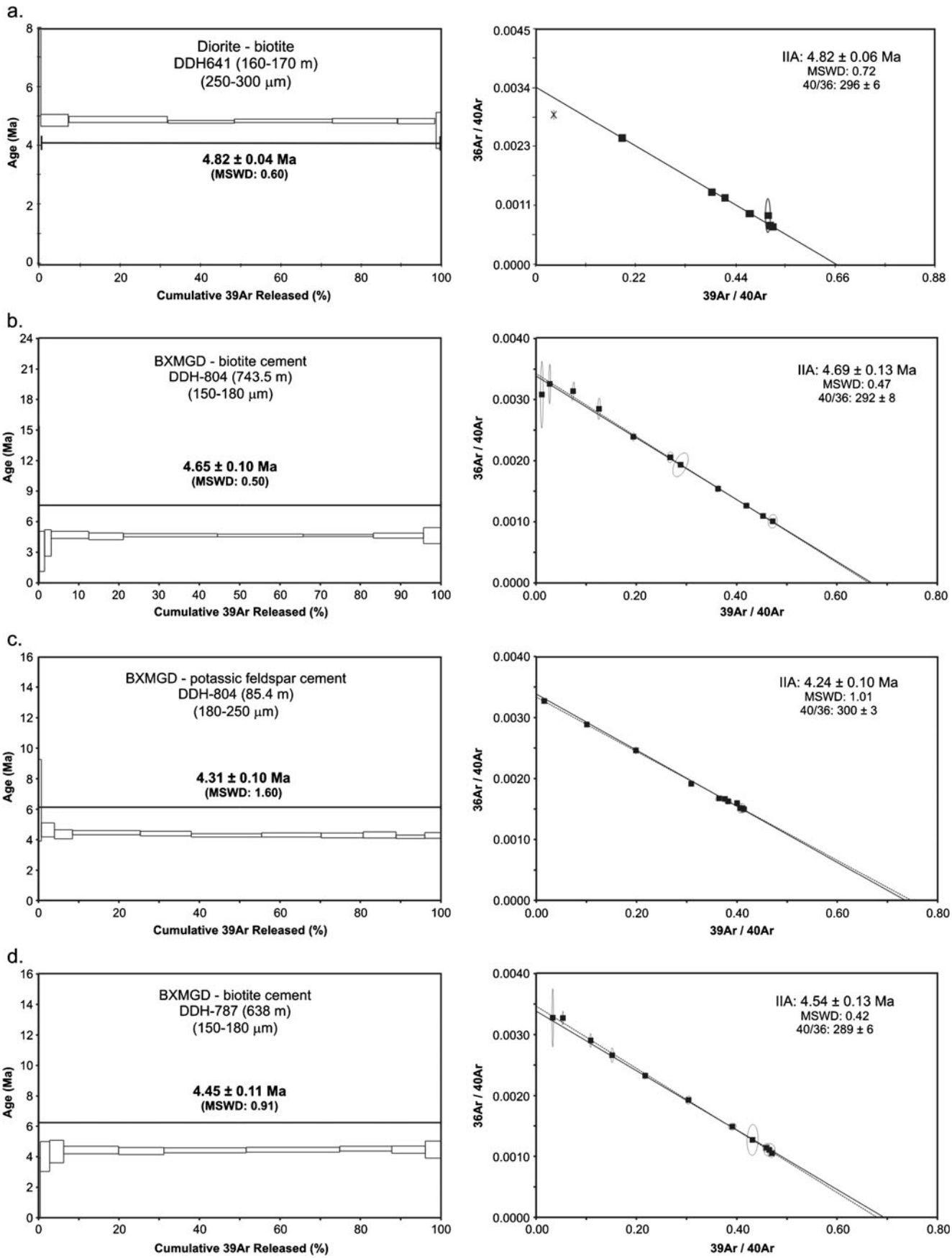
a.
Diorite - biotite
DDH641 (160-170 m)
(250-300 μm)
4.82 ± 0.04 Ma
(MSWD: 0.60)
Age (Ma)
Cumulative 39Ar Released (%)
IIA: 4.82 ± 0.06 Ma
MSWD: 0.72
40/36: 296 ± 6
36Ar / 40Ar
39Ar / 40Ar
b.
BXMGD - biotite cement
DDH-804 (743.5 m)
(150-180 μm)
4.65 ± 0.10 Ma
(MSWD: 0.50)
Age (Ma)
Cumulative 39Ar Released (%)
IIA: 4.69 ± 0.13 Ma
MSWD: 0.47
40/36: 292 ± 8
36Ar / 40Ar
39Ar / 40Ar
c.
BXMGD - potassic feldspar cement
DDH-804 (85.4 m)
(180-250 μm)
4.31 ± 0.10 Ma
(MSWD: 1.60)
Age (Ma)
Cumulative 39Ar Released (%)
IIA: 4.24 ± 0.10 Ma
MSWD: 1.01
40/36: 300 ± 3
36Ar / 40Ar
39Ar / 40Ar
d.
BXMGD - biotite cement
DDH-787 (638 m)
(150-180 μm)
4.45 ± 0.11 Ma
(MSWD: 0.91)
Age (Ma)
Cumulative 39Ar Released (%)
IIA: 4.54 ± 0.13 Ma
MSWD: 0.42
40/36: 289 ± 6
36Ar / 40Ar
39Ar / 40Ar

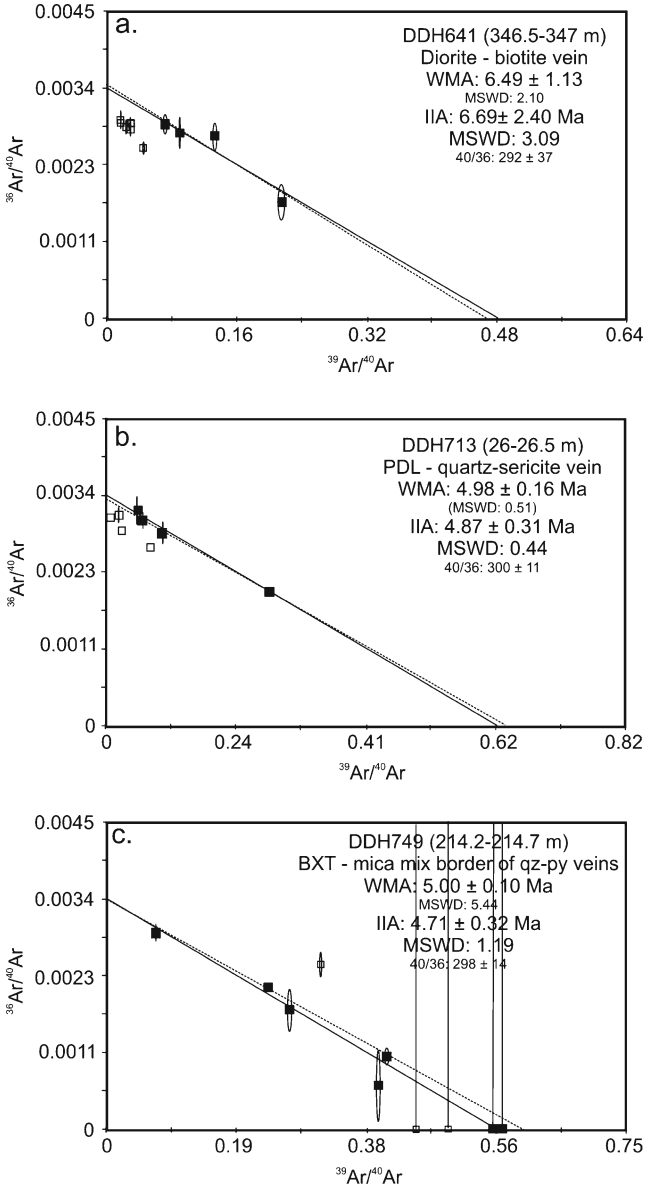

Fig. 9 Inverse isochron diagrams of veins of the San Luís sector. **a** biotite vein in diorite, **b** quartz–sericite vein in Don Luís porphyry and **c** mica rim of quartz–sericite–pyrite vein in tourmaline breccia

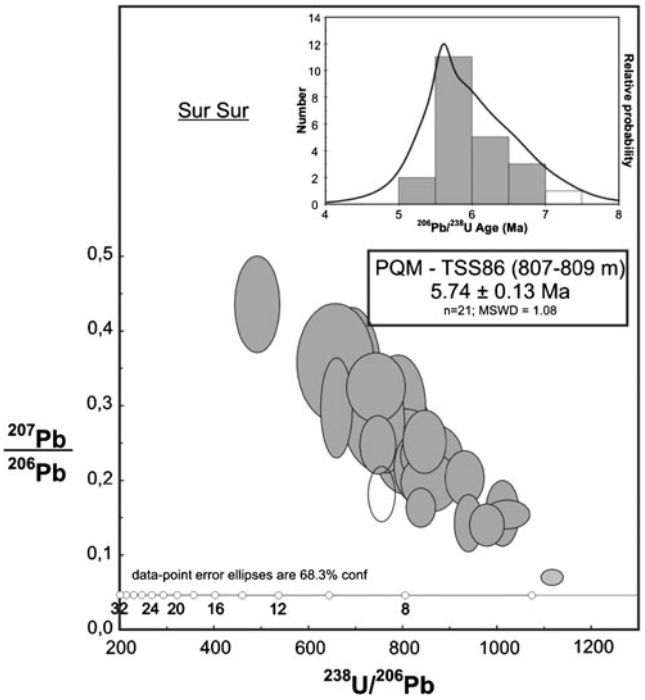

Fig. 10 Tera Wasserburg U/Pb SHRIMP II analyses of quartz monzonite porphyry of the Sur Sur sector. In the histogram, *gray bars* represent numbers of zircon analyses included and *white bars* and ellipsis not included in the age calculation

the Río Blanco sector represents the oldest molybdenite age obtained in this study (Fig. 14a). However, a second "B" vein from the Río Blanco sector is younger than all molybdenite "C" and "E" vein ages from the Sur Sur sector (Fig. 14c). It is noteworthy that molybdenite ages are generally older, the higher their topographic position. Since the youngest "E" vein type of Sur Sur is intermediate in age to all other Re–Os data, it suggests that Mo-mineralisation has a distinct and sector-related as well as diachronic occurrence. It can be outlined that the geochronologic data set might indicate that mineralisation started in the Río Blanco sector, followed by the southernmost Sur Sur and terminated in the central Don Luis sector (Figs. 2b and 14a–c). Furthermore, the heat source of the entire mineralisation event at Río Blanco may have been centred in the Don Luis sector at the end of the hydrothermal history. This would have generated a high-temperature aureole between 4.5 and a 5.5 Ma at that location which resulted in the youngest Mo-vein ages. However, the age tendencies may be an artefact of the still limited data set of only ten molybdenite vein ages. Younger or older events might not have been recognised until now.

New $^{40}Ar/^{39}Ar$ plateau and inverse isochron ages for hydrothermal biotite and K-feldspar range from 5.54 to 4.57 Ma at Río Blanco, from 4.65 to 4.24 Ma at Don Luis, and from 5.14 to 4.42 Ma at Sur Sur (omitting one high-error biotite date; Fig. 13). All dated samples represent intense K-silicate alteration and "A"-type veining (Gustafson and Hunt 1975).

Phyllic alteration was less covered by the $^{40}Ar/^{39}Ar$ method but quartz–sericite vein ages are tentatively oldest in the Río Blanco sector (5.89 Ma, $n=1$), followed by Sur

Fig. 11 $^{40}Ar/^{39}Ar$ age spectra and inverse isochron diagrams of **a** K-feldspar aplite in diorite, **b** feldspar "flooding" event in Cascada granodiorite, **c** K-feldspar vein in tourmaline breccia, **d** K-feldspar vein in tourmaline breccia, **e** biotite cement in magmatic breccia, **f** K-feldspar cement of magmatic breccias and **g** K-feldspar vein in magmatic breccia ▶

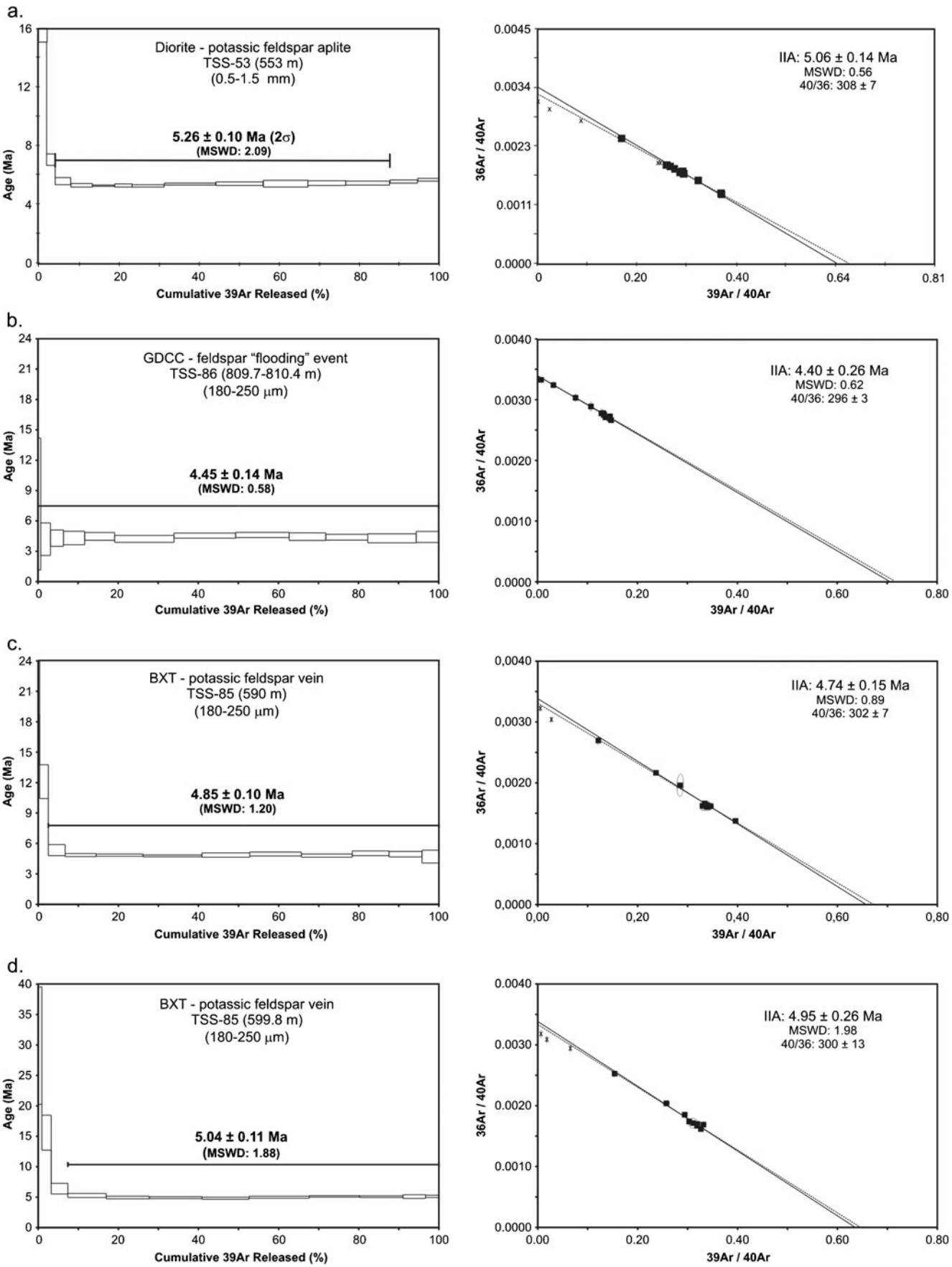
a.
Diorite - potassic feldspar aplite
TSS-53 (553 m)
(0.5-1.5 mm)
5.26 ± 0.10 Ma (2σ)
(MSWD: 2.09)
Age (Ma)
Cumulative 39Ar Released (%)
IIA: 5.06 ± 0.14 Ma
MSWD: 0.56
40/36: 308 ± 7
36Ar / 40Ar
39Ar / 40Ar
b.
GDCC - feldspar "flooding" event
TSS-86 (809.7-810.4 m)
(180-250 μm)
4.45 ± 0.14 Ma
(MSWD: 0.58)
Age (Ma)
Cumulative 39Ar Released (%)
IIA: 4.40 ± 0.26 Ma
MSWD: 0.62
40/36: 296 ± 3
36Ar / 40Ar
39Ar / 40Ar
c.
BXT - potassic feldspar vein
TSS-85 (590 m)
(180-250 μm)
4.85 ± 0.10 Ma
(MSWD: 1.20)
Age (Ma)
Cumulative 39Ar Released (%)
IIA: 4.74 ± 0.15 Ma
MSWD: 0.89
40/36: 302 ± 7
36Ar / 40Ar
39Ar / 40Ar
d.
BXT - potassic feldspar vein
TSS-85 (599.8 m)
(180-250 μm)
5.04 ± 0.11 Ma
(MSWD: 1.88)
Age (Ma)
Cumulative 39Ar Released (%)
IIA: 4.95 ± 0.26 Ma
MSWD: 1.98
40/36: 300 ± 13
36Ar / 40Ar
39Ar / 40Ar

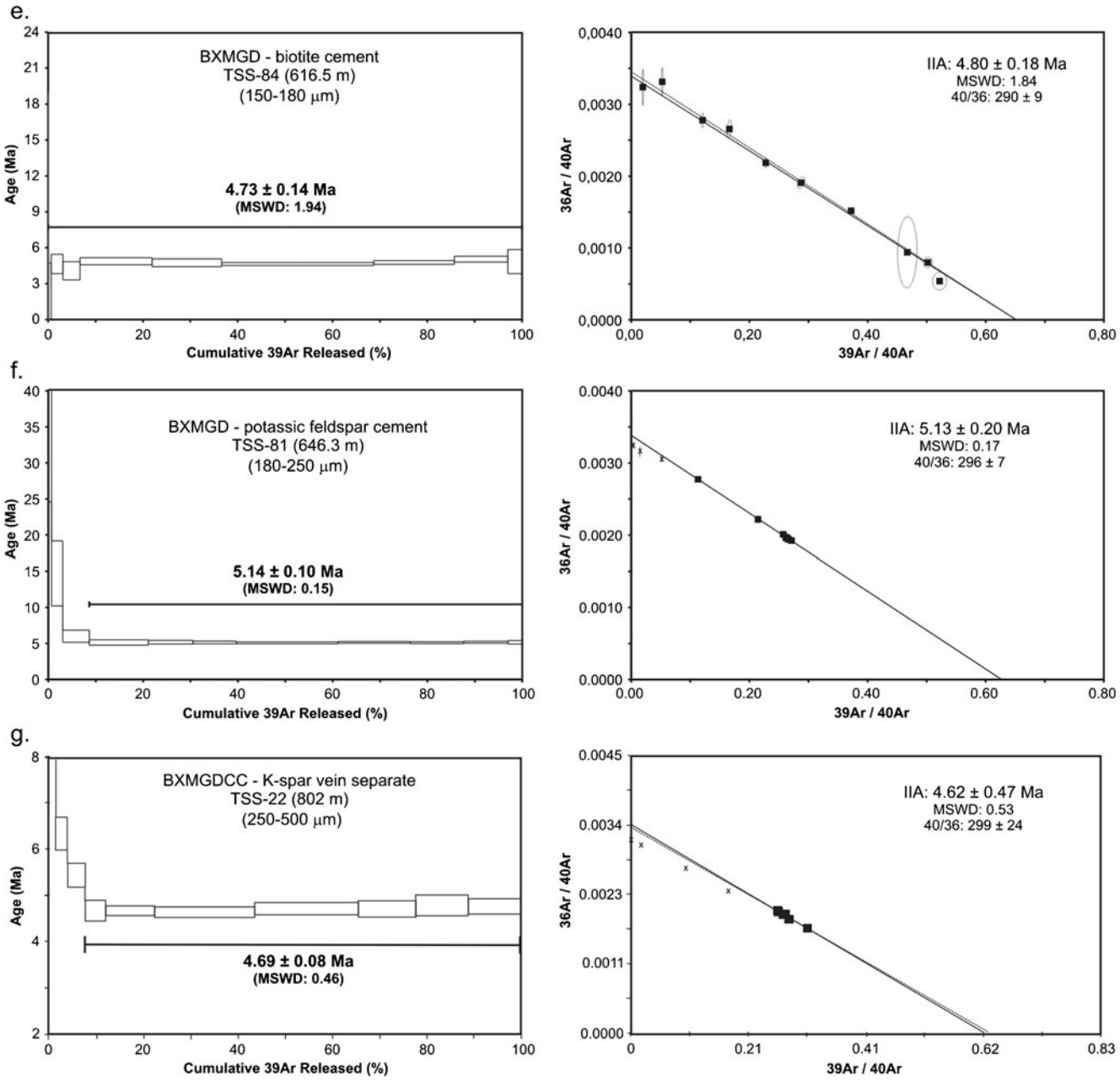

Fig. 11 (continued)

Sur (5.49 Ma, $n=1$) and youngest in the Don Luis sector (4.37–4.87 Ma, $n=3$). The new phyllic alteration ages are visibly older than the relative probability peak at 4.38 Ma indicated in Deckart et al. (2005). However, the previous data set contained only the two youngest ages of the Don Luis sector. Furthermore, phyllic alteration is overlapping with the hydrothermal potassic alteration event (Figs. 13 and 14).

Although coinciding with the Re–Os dates in all three sectors, most of the 40Ar/39Ar ages are younger than the Re–Os dates of paragenetically younger vein types (Fig. 13).

It is impossible to group $^{40}Ar/^{39}Ar$ ages and recognise different mineralisation pulses which affected the Cu(–Mo) porphyry deposit since the obtained ages cluster around a certain statistical probability which is geologically meaningless and does not date hydrothermal alteration events but might indicate the age of thermal resetting. On the other hand, if temperatures below 350–400°C caused resetting, only $^{40}Ar/^{39}Ar$ ages would have been affected, leaving the Re–Os isotope system unchanged. Consequently, Re–Os ages likely represent valid mineralisation ages. However, since individual Re–Os ages are not overlapping in age

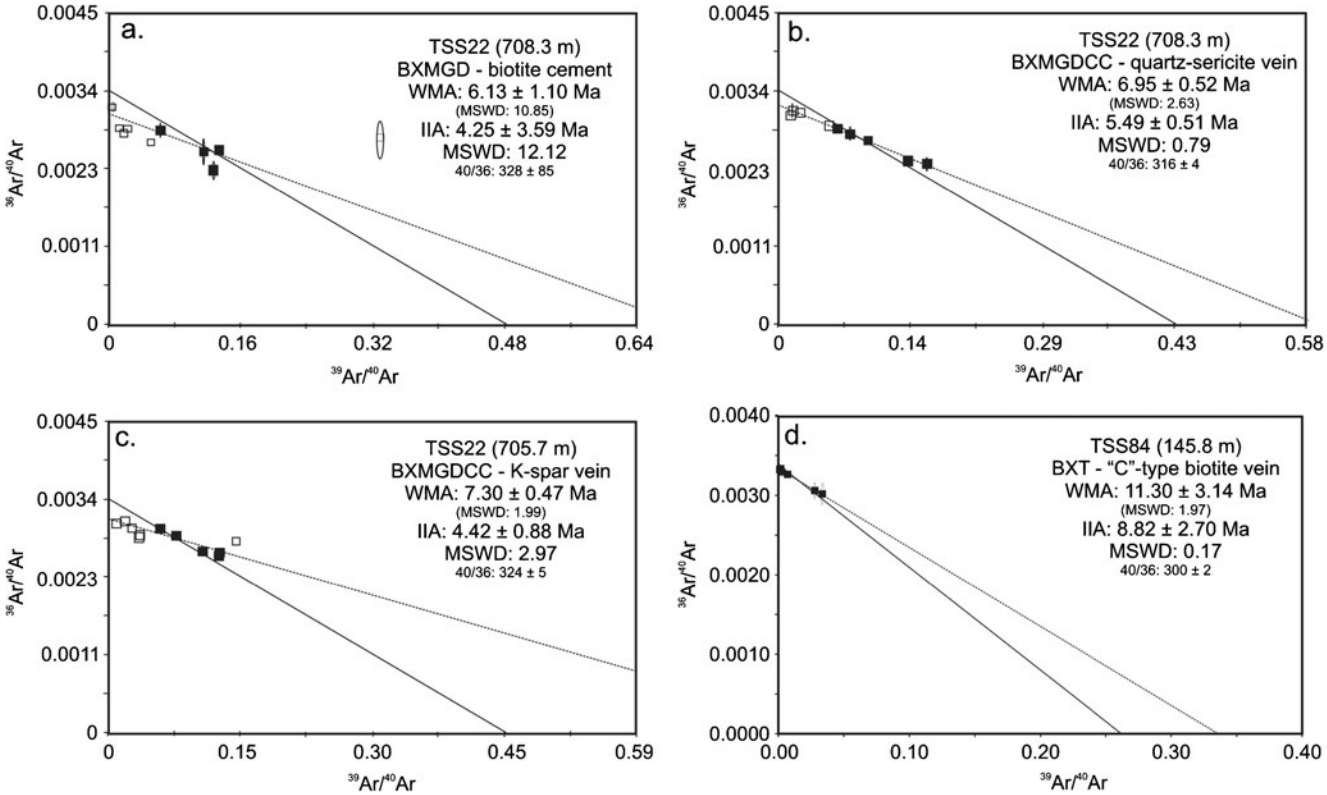

Fig. 12 Inverse isochron diagrams of veins and cement of the Sur Sur sector. **a** biotite cement, **b** quartz–sericite vein **c** K-feldspar vein in magmatic breccia and **d** C-type biotite vein in tourmaline breccia

(errors are 0.5 % of the individual age) it would be an overestimation to interpret each age as a single hydrothermal event (Figs. 13 and 14). The Re–Os data can be statistically grouped into three age intervals; the youngest ranges between 4.50 and 5.11 Ma and mainly represents the Don Luis sector (Fig. 14b), the intermediate group ranges from 5.40 to 5.94 Ma, and the oldest group represents ages older than 6.26 Ma, age groups which include the ages obtained by Mathur et al. (2001). The intermediate and oldest age groups are represented in the Río Blanco (Fig. 14a) and Sur Sur (Fig. 14c) sectors, which confirm the same spatial age group distribution as seen with the new $^{40}Ar/^{39}Ar$ ages.

In a regional context, recent work by Yañez et al. (2002) and the suggested causal link in time and space with flat slab subduction supported by K–Ar and $^{40}Ar/^{39}Ar$ data from Skewes et al. (2002) promote the interpretation that the apparent southward younging of mineralisation is related to changes in arc magmatism due to the southward propagating locus of the Juan Fernandez ridge subduction (Skewes and Stern 1994). However, Kay and Mpodozis (2001) suggested that mineralisation at the El Teniente deposit lies outside the 200 km swath of the ridge centre and therefore could not have been directly influenced by the ridge subduction. Le Roux et al. (2005) attributed uplift of the Carrizalillo (~29°S) and Tongoy (~30°S) areas between 11.8 and 7.7 Ma and 10.5 and 6.9 Ma, respectively, to the approach and subduction of the Juan Fernández Ridge. This observation implies that for the three Mio-Pliocene porphyry Cu(-Mo) deposits in central Chile the Juan Fernández Ridge subduction was not a direct trigger of mineralisation considering a southward migration not exceeding 25 km/Ma as postulated by Yañez et al. (2002). In other words, Los Pelambres (32° S) at 11.2–10.4 Ma (Bertens et al. 2003), Río Blanco-Los Bronces (33° S) at 6.4–4.5 Ma (Deckart et al. 2005; and this work) and El Teniente (34° S) at 6–4 Ma (Maksaev et al. 2004; Cannell et al. 2005) formed at the same time when uplift through the arrival of the Juan Fernandéz Ridge was ascribed about 200 km further north. Charrier et al. (2002) proposed that it is not yet possible to determine if collision had a local effect or if plate reorganisation affected the late Cenozoic tectonics of the entire continental margin of the Central Andes. According to Kay et al. (2005), ridge subduction is only a minor perturbation in a much larger geodynamic scheme driven by plate interactions or mantle flow. Stern and Skewes (2005) and Skewes et al. (2005) are sustaining their argumentation on historical K–Ar ages and continue discussions about a direct link of ridge subduction and mineralisation in the Central Andes.

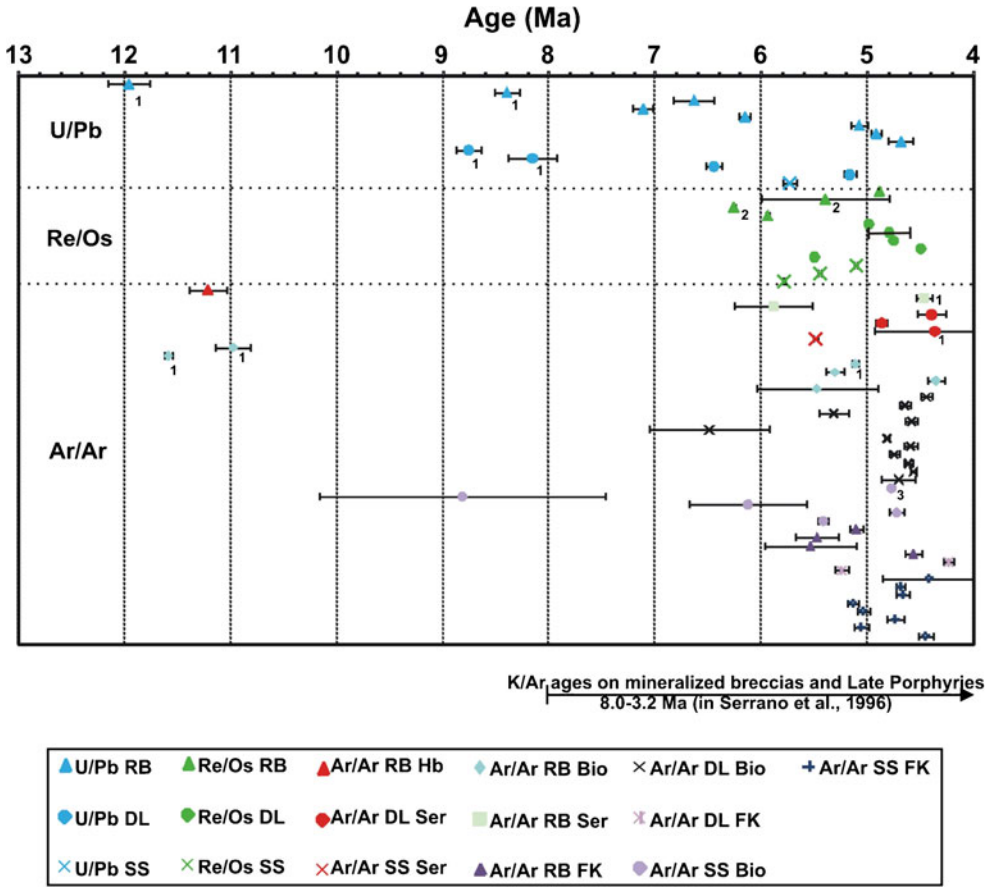

Fig. 13 Entire geochronological data set for Río Blanco, Don Luis and Sur Sur sectors, Rio Blanco-Los Bronces prophyry Cu(–Mo) deposit. Ages from 1 Deckart et al. (2005), 2 Mathur et al. (2001), 3 Frikken et al. (2005) and this study. *RB* Río Blanco, *DL* Don Luis, *SS* Sur Sur, *Hb* hornblende, *Ser* sericite, *FK* K-feldspar, *Bio* biotite. Errors are quoted as 1σ

Conclusions

The older magmatic dioritic pulse of the San Francisco batholith confirmed recently published U–Pb data and indicates for the diorite an age range from 8.8 to 8.2 Ma (Fig. 13). The entire U–Pb data set suggests that the porphyry intrusions are characterised by an age range and single age determinations are unlikely to reflect individual magmatic pulses. U–Pb ages are ranging for the Quartz Monzonite porphyry between 7.7 and 6.1 Ma (exception in the Sur Sur sector, 5.74±0.13 Ma), between 5.8 and 5.2 Ma for the Feldspar porphyry, and from 5.2 to 5.0 Ma for the Don Luis porphyry. The post-mineralisation La Copa rhyolite plug (4.69±0.23 Ma, U–Pb SHRIMP II) in addition to the dacite plug (4.92±0.1 Ma; U–Pb SHRIMP II; Deckart et al. 2005) could be the triggers of the thermal perturbation of the entire Ar–Ar data of the deposit which took place between 5.0 and 4.6 Ma (Fig. 13).

The new Re–Os age data confirm the protracted history of Cu(–Mo) mineralisation inferred by Deckart et al. (2005). Although the 6.3 Ma molybdenite date reported by Mathur et al. (2001) could not be confirmed, it is evident that molybdenite bearing veins were emplaced at least from 5.94 to 4.50 Ma in this giant hydrothermal system (Fig. 13), i.e. a time-span of ca. 1.5 Ma However, the Mo-rich vein events may not accurately constrain the age of the bulk of the Mo–Cu mineralisation of the deposit. The only breccia cement (Mo rich) which was dated is the single age of 6.26±0.04 Ma from Mathur et al. (2001). The dated breccia hosts a considerable proportion of the Cu budget (Serrano et al. 1996). We can therefore conclude that Cu–Mo mineralisation persisted for at least 2 Ma overall (see Deckart et al. 2005). At least in the Don Luis sector, "C" veins with chlorite-sericite selvages predated veins with "transitional" or "B"-vein characteristics (cf. Gustafson and Hunt 1975). Whereas "Late Porphyry" intrusions apparently commenced earliest in the northern, Río Blanco sector (Fig. 14a), the Re–Os dates demonstrate extensive temporal overlap of Mo mineralisation in the Río Blanco, Don Luis and Sur Sur sectors (Fig. 14a–c). It is implicit that, as proposed by Deckart et al. (2005), "Late Porphyry" magmatism was not directly responsible for the major Cu–Mo mineralisation. It is rather suggested that mineralisation records an event in a deeper, unexposed parental magma chamber possibly independent of the "Late Porphyry" magmatism. The new, paragenetically constrained Re–Os dates support our previous conclusion that ore formation in the Río Blanco cluster was essentially synchronous with that at El Teniente, about 110 km to the south. Thus, molybdenite deposition is shown to have persisted at least from 5.94 to 4.50 Ma (extended to 6.3 Ma according to Mathur et al.

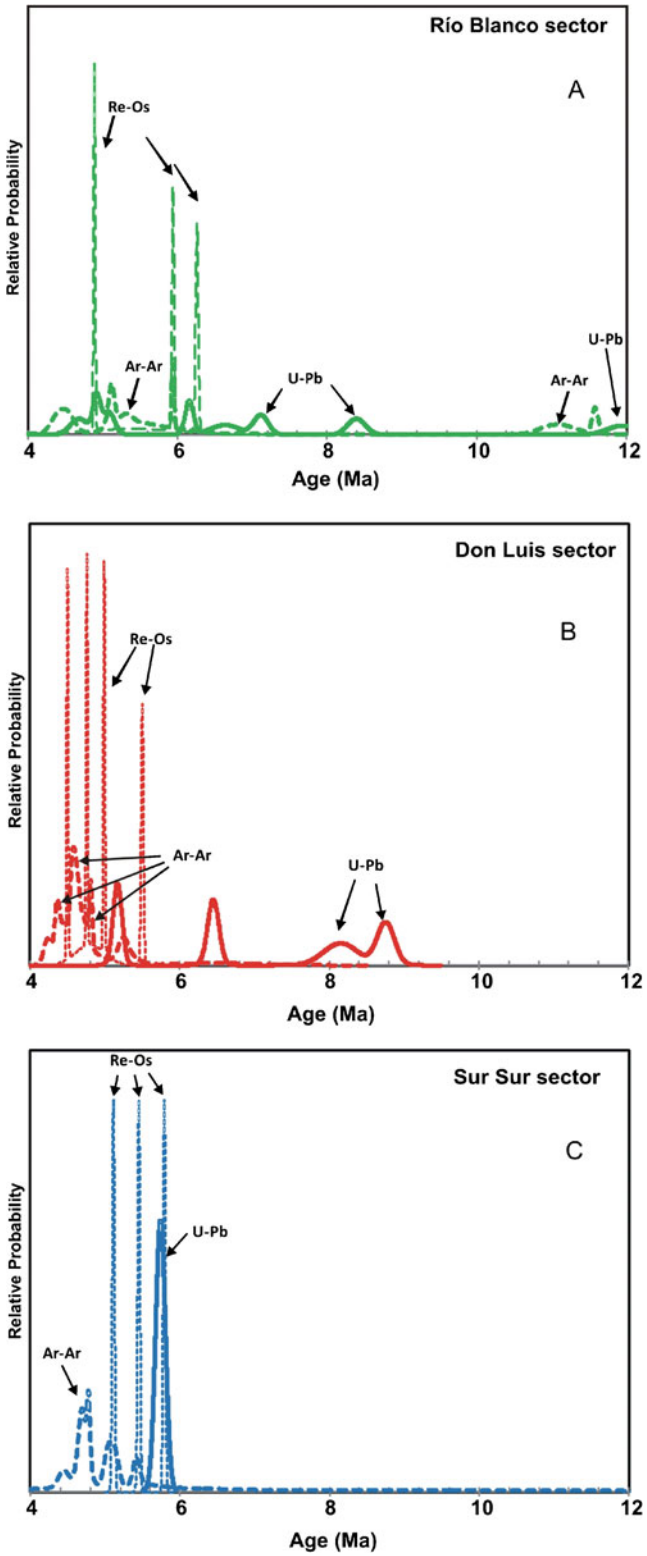

Fig. 14 Age distribution of the entire geochronologic data set summarised by sector: **a** Río Blanco, **b** Don Luis and **c** Sur Sur. Ages included in the data set are from Mathur et al. (2001), Deckart et al. (2005), Frikken et al. (2005) and this study. Ages are given at the 2σ level

2001) in the eastern and southern centres (Fig. 13) of the Río Blanco-Los Bronces mine, whereas Cannell et al. (2005) define a spread in molybdenite ages of 4.70 to 5.89 Ma for El Teniente, an interval extended to 4.42 Ma by the data of Mathur et al. (2001).

Although overlapping with the Re–Os dates, the new $^{40}Ar/^{39}Ar$ plateau and inverse isochron dates for hydrothermal K-silicate minerals are largely too young to record the age of early, high-temperature mineralisation. Further, the apparent age ranges for biotites and K-feldspars in each centre (Fig. 13; Río Blanco, 4.36–5.31 Ma; Don Luis, 4.24–4.65 Ma; and Sur Sur, 4.45–5.14 Ma) have no clear paragenetic connotation. We therefore reaffirm our earlier conclusion (Deckart et al. 2005) that all, or the large majority of the $^{40}Ar/^{39}Ar$ dates for hydrothermal minerals in the wider Río Blanco porphyry cluster record reheating by either the youngest member of the Late Porphyry suite, i.e. the Don Luis porphyry (5.08–5.23 Ma in the Río Blanco sector) or, more extensively, the 4.92 Ma dacite and 4.69 Ma rhyolite plugs (Fig. 2b).

On a regional scale, the enlarged geochronological data set, supported by the inferred position of the Juan Fernandez Ridge at the latitude of ~30° S (Bahia Tongoy) during the Late Miocene (Le Roux et al. 2005, 2006)), shows clearly that the subduction of the ridge could not have triggered the mineralisation between 6.3 and 4.4 Ma, neither in the Río Blanco-Los Bronces nor in the El Teniente (~110 km further south) Cu–Mo districts. If ridge subduction initiated the flattening of the subduction angle, our geochronological data suggest that the youngest behmothian (sensu Clark 1993) very large copper deposits in the central Andes formed slightly before and maybe partly during this geodynamic event. Furthermore, with the herein presented data and those from Deckart et al. (2005), we can discard that there is a causal link in time and space between flat slab, southward migration of the locus of subduction of the Juan Fernandez Ridge and mineralisation between 32° and 34° S as emphasised in Yañez et al. (2002) and Skewes and Stern (1994).

Acknowledgements The authors would like to thank Andina Division of CODELCO-Chile for funding the second geochronological project and permitting publication of the data. Special thanks go to Luis Serrano, former Administrator of Exploration and Mineral Resources, for supporting this investigation, and mine geologists Humberto Ortega, Augusto Mont, Nicolas Pizarro and Francisco Fuentes for their stimulating discussions. At Oregon State University, Robert Duncan and at Arizona University, Fernando Barra, carried out analytical $^{40}Ar/^{39}Ar$ and Re–Os work, respectively. Juan Vargas is thanked for mineral separation in the facilities of the Geology Department, Universidad de Chile. We would like to thank reviewers Thomas Bissig, Richard Tosdal and Regina Baumgartner for their helpful comments on the earlier version of the manuscript. Parts of the U–Pb and $^{40}Ar/^{39}Ar$ geochronological analyses were financed through the Chilean grant DID-I-04-2/2001.

References

Bertens A, Deckart K, Gonzalez A (2003) Geocronología U–Pb, Re–Os, y 40Ar/39Ar del pórfido Cu–Mo Los Pelambres, Chile Central. X. Congreso Geológico Chileno, Concepción, 2003 (CD-ROM): 5

Cannell J, Cooke DR, Walshe JL, Stein H (2005) Geology, mineralization, alteration, and structural evolution of the El Teniente porphyry Cu–Mo deposit. Econ Geol 100:979–1003

Charrier R, Baeza O, Elgueta S, Flynn JJ, Gans P, Kay SM, Muñoz N, Wyss AR, Zurita E (2002) Evidence for Cenozoic extensional basin development and tectonic inversion south of the flat-slab segment, southern Central Andes, Chile (33–36° S.L.). J S Am Earth Sci 15:117–139

Chesley JT (1999) Integrative geochronology of ore deposits: New insights into the duration and timing of hydrothermal circulation. In: Lambert DD, Ruiz J (eds) Application of radiogenic isotopes to ore deposit research and exploration. Rev Econ Geol 12: 115–141

Clark AH (1993) Are outsize porphyry copper deposits either anatomically or environmentally distinct? In: Whiting BH, Hodgson CJ, Mason R (eds) Giant ore deposits. Soc Econ Geol Spec Publ 2: 213–283

Creaser RA, Erdmer P, Stevens RA, Grant SL (1993) Tectonic affinity of Nisutlin and Anvil assemblage strata from the Teslin Tectonic Zone, northern Canadian Cordillera: constraints from neodymium isotope and geochemical evidence. Tectonics 16:107–121

Deckart K, Clark AH, Aguilar C, Vargas R, Bertens A, Mortensen J, Fanning M (2005) Magmatic and hydrothermal chronology of the giant Río Blanco porphyry copper deposit, Central Chile: implications of an integrated U–Pb and ^{40}Ar–^{39}Ar database. Econ Geol 100:905–934

Deckart K, Godoy E, Bertens A, Jeréz D, Saeed A (2010) Barren Miocene granitoids in the Central Andean metallogenic belt, Chile: geochemistry and Nd–Hf and U–Pb isotope systematics. Andean Geol 37:1–31

Dilles JH, Einaudi MT (1992) Wall-rock alteration and hydrothermal flow paths about the Ann-Mason porphyry copper deposit—a 6-km vertical reconstruction. Econ Geol 87:1963–2001

Dodson MH (1973) Closure temperature in cooling geochronological and petrological systems. Contrib Mineral Petrol 40:259–274

Frikken PH, Cooke DR, Walshe JL, Archibald D, Skarmeta J, Serrano L, Vargas R (2005) Mineralogical and isotopic zonation in the Sur-Sur tourmaline breccia, Río Blanco-Los Bronces Cu–Mo deposit, Chile—implications for ore genesis. Econ Geol 100:935–961

Gustafson LB, Hunt JP (1975) The porphyry copper deposit at El Salvador, Chile. Econ Geol 70:857–912

Gustafson LB, Quiroga J (1995) Patterns of mineralization and alteration below the porphyry copper orebody at E1 Salvador, Chile. Econ Geol 90:2–16

Harrison TM, McDougall I (1982) The thermal significance of potassium feldspar K–Ar ages inferred from ^{40}Ar/^{39}Ar age spectrum results. Geochim Cosmochim Acta 46:1811–1820

Kay SM, Mpodozis C (2001) Central Andean ore deposits linked to evolving shallow subduction systems and thickening crust. Geol Soc Am (GSA) Today 11(3):4–9

Kay SM, Godoy E, Kurtz A (2005) Episodic arc migration, crustal thickening, subduction erosion, and magmatism in the south-central Andes. Geol Soc Am Bull 117:67–88

Le Roux JP, Gomez CA, Olivares DM, Middleton H (2005) Determining the Neogene behavior of the Nazca plate by geohistory analysis. Geology 33:165–168

Le Roux JP, Olivares DM, Nielsen SN, Smith ND, Middleton H, Fenner F, Ishman SE (2006) Bay sedimentation as controlled by regional crustal behaviour, local tectonics and eustatic sea-level changes: Coquimbo Formation (Miocene–Pliocene), Bay of Tongoy, central Chile. Sed Geol 184:133–153

Ludwig KR (1999) User's manual for Isoplot/Ex, Version 2.10, A geochronological toolkit for Microsoft Excel: Berkeley Geochronology Center. Spec Publ 1a

Ludwig KR (2000) SQUID 1.00, A user's manual. Berkeley Geochronology Center, Spec Publ 2.

Maksaev V, Munizaga F, McWilliams M, Mathur R, Ruiz J, Zentilli M (2004) New chronology for El Teniente, Chilean Andes, from U–Pb, ^{40}Ar/^{39}Ar, Re–Os, and fission-track dating: Implications for the evolution of a supergiant porphyry Cu–Mo deposit. Soc Econ Geol Spec Publ 11:15–54

Masterman GJ, Cooke DR, Berry RF, Walshe JL, Lee AW, Clark AH (2005) Fluid chemistry, structural setting, and emplacement history of the Rosario Cu–Mo porphyry and Cu-Ag-Au epithermal veins, Collahuasi district, northern Chile. Econ Geol 100:835–862

Mathur R, Ruiz JR, Munizaga FM (2001) Insights into Andean metallogenesis from the perspective of Re–Os analyses of sulphides. South American Isotope Conference, (CD-ROM). SERNAGEOMIN, Chile, p 4

Mining Journal (2009) Anglo unveils major new deposits. Exploration & Development. The Mining Industry's Weekly Newspaper Online 07/08/2009: p 3

Nägler T, Frei R (1997) 'Plug-in' Os distillation. Schweiz Mineral Petrogr Mitt 77:123–127

Paces JB, Miller JD (1993) Precise U–Pb ages of Duluth Complex and related mafic intrusions, northeastern Minnesota: geochronological insights to physical, petrogenetic, paleomagnetic, and tectonomagmatic process associated with the 1.1 Ga Midcontinent Rift System. J Geophys Res 98:13,997–14,013

Quirt GS (1972) A potassium-argon geochronological investigation of the Andean mobile belt of north-central Chile. Unpublished Ph.D. thesis, Queens' University, Kingston, Ontario, Canada, 240 pp

Quirt GS, Clark AH, Farrar E, Sillitoe RH (1971) Potassium-argon ages of porphyry copper deposits in northern and central Chile. Econ Geol 67:980–981

Rivano S, Godoy E, Vergara M, Villarroel R (1990) Redefinición de la Formación Farellones en la Cordillera de los Andes de Chile Central (32–34° S). Rev Geol Chile 17(2):205–214

Serrano L, Vargas R, Stambuk V, Aguilar C, Galeb M, Holmgren C, Contreras A, Godoy S, Vela L, Skewes MA, Stern CR (1996) The Late Miocene to early Pliocene Río Blanco-Los Bronces copper deposit, central Chilean Andes. In: Camus F, Sillitoe RH, Petersen R (eds) Andean copper deposits: new discoveries, mineralization, styles and metallogeny. Soc Econ Geol, Spec Publ 5: 119–130

Shirey SB, Walker RJ (1995) Carius tube digestion for low-blank rhenium-osmium analysis. Anal Chem 67:2136–2141

Skewes MA, Stern CR (1994) Tectonic trigger for the formation of Late Miocene Cu-rich breccias pipes in the Andes of central Chile. Geology 22:551–554

Skewes MA, Arévalo A, Floody R, Zúñiga H, Stern CR (2002) The giant El Teniente breccia deposit: hypogene copper distribution and emplacement. Soc Econ Geol Spec Publ 9:299–332

Skewes MA, Arévalo A, Floody R, Zúñgiga P, Stern CR (2005) The El Teniente megabreccia deposit, the world's largest copper deposit. In: Porter TM (ed) Super porphyry copper & gold deposits—a global perspective. PGC Publishing, Adelaide, Australia, pp 83–114

Steiger RH, Jäger E (1977) Subcomission on geochronology: convention on the use of decay constants in geo- and cosmochronology. Earth Planet Sci Lett 36:359–362

Stern CR, Skewes MA (2005) Origin of giant Miocene and Pliocene Cu–Mo deposits in central Chile: role of ridge subduction, decreased subduction angle, subduction erosion, crustal thickening and long-lived, batholith sized, open-system magma chambers.

In: Porter TM (ed) Super porphyry copper & gold deposits—a global perspective. PGC Publishing, Adelaide, Australia, pp 65–82

Suzuki K, Shimizu H, Masuda A (1996) Re–Os dating of molybdenites from ore deposits in Japan; implication for closure temperature of Re–Os system for molybdenite and cooling history of molybdenum ore deposits. Geochim Cosmochim Acta 60:3151–3159

Tera F, Wasserburg GJ (1972) U-Th-Pb systematic in three Apollo 14 basalts and the problem of initial Pb in lunar rocks. Earth Planet Sci Lett 14:281–304

Warnaars FW, Holmgrem C, Barassi S (1985) Porphyry copper and tourmaline breccias at Los Bronces-Río Blanco, Chile. Econ Geol 80:1544–1565

Williams IS (1998) U–Th–Pb geochronology by ion microprobe. In: McKibben MA, Shanks III WC, Ridley WI (eds) Applications of microanalytical techniques to understanding mineralizing processes. Rev Econ Geol 7: 1–35

Yañez G, Cembrano J, Pardo M, Ranero C, Selles D (2002) The Challenger–Juan Fernández–Maipo major tectonic transition of the Nazca–Andean subduction system at 33–34°: geodynamic evidence and implications. J S Am Earth Sci 15:23–38